2017-08-07

Energy Efficiency Improvement of VFD-Motor-Pump/Fan Systems

Koosha Kiamehr
University of Miami, koosha.kia@gmail.com

UNIVERSITY OF MIAMI

ENERGY EFFICIENCY IMPROVEMENT OF VFD-MOTOR-PUMP/FAN SYSTEMS

By

Koosha Kiamehr

A DISSERTATION

Submitted to the Faculty
of the University of Miami
in partial fulfillment of the requirements for
the degree of Doctor of Philosophy

Coral Gables, Florida

August 2017

UNIVERSITY OF MIAMI

A dissertation submitted in partial fulfillment of
the requirements for the degree of
Doctor of Philosophy

ENERGY EFFICIENCY IMPROVEMENT OF VFD-MOTOR-PUMP/FAN SYSTEMS

Koosha Kiamehr

Approved:

_____ Gang Wang, Ph.D. Assistant Professor of Architectural Engineering	_____ Wangda Zuo, Ph.D. Assistant Professor of Architectural Engineering
_____ David Chin, Ph.D. Professor of Environmental Engineering	_____ Guillermo Prado, Ph.D. Dean of the Graduate School
_____ Hongtan Liu, Ph.D. Professor of Mechanical Engineering	

KIAMEHR, KOOSHA (Ph.D., Civil Engineering)
Energy Efficiency Improvement of (August 2017)
VFD-Motor-Pump/Fan Systems

Abstract of a dissertation at the University of Miami.

Dissertation supervised by Professor Gang Wang.
No. of pages in text. (88)

Pumps and fans, which are driven by electrical motors, are the integral parts of heating, ventilating and air conditioning (HVAC) systems and a lot of research have been dedicated to improve the efficiency of them. Recent developments, increased the complexity of these systems, made them hard to study and model. To improve the energy efficiency of the system, variable frequency drives (VFDs) are widely applied on the electric motors of pumps and fans to reduce energy consumption. VFDs have two functions: reducing frequency to reduce the speed and match the reduced load and reducing voltage to reduce motor power. VFDs change voltage and frequency together, and they use some preset ratios to do that. The ratio of voltage to frequency squared, called the squared ratio, is applied for centrifugal fans and pumps, which are considered to have a cubic correlation between the motor load and speed. VFD manufacturers did not give any simulation or experimental supporting data for the recommended preset ratios. Faults are another great factor which causes extra energy consumption in the system and fan belt slippage and pressure setpoint override faults are two of the most common faults regarding pumps and fans. Currently, these faults have to be detected by either data driven, model-based or rule-based fault detection and diagnosis (FDD) approaches. For FDD, model based approach generally require high computational time,

which makes it unsuitable for real time applications. Rule based approaches used physical flow meters which are either expensive or inaccurate. Accurate fault detection strategies require flow rate measurements. As mentioned, conventional physical flow meters are not usually accurate and have some installment conditions which makes them unsuitable to be installed right upstream of the pumps and fans. Consequently, virtual flowmeters have been emerged in the recent years but the calibration process for using them is still complicated. The first purpose of this study is to investigate energy efficient voltage-frequency ratios of VFDs driving the induction motors of fans and pumps. First, equivalent motor circuit is used to simulate the motor efficiency, then experiments are designed to validate the results. The second purpose of this work is to develop a hybrid (combination of rule based and data driven) FDD approach which can be implemented in building automation system (BAS). Experiential rules are developed based on affinity laws and head-flowrate relationship and used to identify faults and experimental data are used to calibrate the developed relation. Finally, the implementation of the existing virtual flowmeter technology is simplified and improved by making changes in calibration parameters which makes the calculation process easier.

Table of Contents

List of Figures

List of Abbreviations

a-d = constants

f = VFD frequency, hz

$\bar{f}$ = VFD relative frequency

H = pump/fan head, Pa, Psi, inch ofwater or feet of water

H_{sp} = pressure setpoint, Pa or ft of water

I_1 = stator or input current. A

I_2 = rotor or load current, A

Q = pump/fan flow rate, L/s, gpm or CFM

R_1 = stator winding resistance, ohm

R_2 = rotor winding resistance, ohm

R_c = core loss resistance, ohm

s =motor slip

S = overall resistance factor with respect to flow rate, $Pa/(m^3/s)^2$ or ft of water/GPM^2

T = motor torque, N.m

V = VFD voltage, V

V_1 = input phase voltage, V

V_2 = rotor or load phase voltage. V

V_m = magnetizing or air gap voltage phase voltage, V

W = motor mechanical load or pump/fan shaft power, kW

W_F = friction loss, kW

W_W = *windage loss, kW*

$W_{F\&W}$ = *mechanical losses, kW*

W_{rotor} = *rotor mechanical output power, kW*

W_{motor} = *motor power, kW*

W_{shaft} = *pump/fan shaft power, kW*

W_{water} = *mechanical work received by water, kW*

X = *total leakage reactance, ohm*

X_1 = *stator leakage reactance, ohm*

X_2 = *rotor leakage reactance, ohm*

X_m = *magnetizing reactance, ohm*

Z = *impedance, ohm*

η = *efficiency*

η_{motor} = *motor efficiency*

η_{pump} = *pump efficiency*

η_{fan} = *fan efficiency*

θ = *phase angle between voltage and current*

ω = *relative pump speed based on the reference speed*

Φ = *magnetizing flux, Wb*

Subscripts

d = *design*

H = *head*

r = *reference*

sp = *setpoint*

W = *power*

Imp = implicit

n = weight factor

Chapter 1: Introduction

Energy is a fundamental requirement for buildings as well as industrial sectors. The alarming rate of increase in the world's population and the economy had an impact with enormous energy consumption (Abdelaziz 2011). Over the years, increased usage of conventional sources for the generation of electrical energy has depleted the energy resources and is causing drastic climatic changes. Furthermore, this will also result in an energy crisis which results in increase in cost of energy as well as a fluctuation in its price. In 2014, 41% of total U.S. energy consumption or about 40 quads (11.7×10^{12} TWh), was consumed in residential and commercial buildings. Heating, ventilating, and air conditioning (HVAC) systems are intensive energy consumers. The investigation of conserving HVAC energy is of great importance because of the increasing awareness of sustainability and environmental protection.

Electric motors, which drive fans and pumps, provide the primary force to recirculate water and air in HVAC systems. In recent years, variable frequency drives (VFDs) have been extensively used in order to reduce the energy consumption of fans and pumps. In this study, the goal is to introduce methods to reduce the energy consumption and improve the performance of VFD-motor-pump/fan systems. The introduced methods can be summarized into three categories:

1. VFD voltage to frequency ratio optimization
2. Fault detection (using VFD outputs and virtual flowmeter)
3. Virtual flowmeter (using VFD outputs)

In which, a virtual flow meter is not an energy efficiency method by itself, but it has been used to develop the proposed methods. In the following each of these methods has been briefly introduced.

1.1 VFD voltage to frequency ratio

Among electric motors, alternating current (AC) three-phase induction motors are extensively used to operate pumps and fans in commercial buildings because of their low cost and consistent operation. AC induction motors rotate at a nearly constant speed slightly different from their synchronous speed by a slip speed. The amount of slip increases roughly proportional to the mechanical load while the synchronous speed is determined by the frequency of power supply and the number of electrical magnetic poles (Hughes 2006). The typical synchronous speed is 3,600, 1,800, 1,200, or 900 rpm in the power systems with a rated frequency of 60 Hz.

The motor mechanical load is dynamic, especially for fans and pumps in HVAC systems. The U.S. Department of Energy (DOE) (2008) presented that during more than 40% of operating hours the motors in industrial applications operate at or below 40% of their rated load. VFDs can convert constant frequency and voltage input power into variable output frequency and voltage to modulate the speed of the connected motor. Since the shaft power to pumps or fans varies as the cube power of motor speed ratio, which is approximately proportional to the VFD output frequency, substantial motor power reduction can be achieved by installing VFDs on pumps or fans. Typically in HVAC systems, VFDs are modulating the fan or pump frequency to maintain a constant pressure (pressure setpoint) in the system. Energy savings of 50% or more were observed when fixed speed systems are modified to allow the motor speed to match variable load

requirements (DOE 2008). The energy savings have been the most interesting benefit to encourage wide applications of VFDs in HVAC industries.

Currently the most common VFD is the pulse width modulation (PWM) type. AC supply voltage is converted into direct current (DC) voltage by a rectifier, then the DC voltage is flattened using filter capacitors in a DC link, and finally the flattened DC voltage is applied to the output load as a series of pulses with varying duration and frequency. The DC voltage pulse is turned on and off at a switching frequency between 1 kHz and 20 kHz to result in an approximately sinusoidal current, which contains harmonics, defined as the irregularities in the sinusoidal wave. The width of the pulse determines the resultant VFD output voltage while the changeover frequency between positive and negative pulses equals the VFD output frequency (DOE 2008, CEATI 2000).

In spite of the energy savings and PF improvement, VFDs, as electrical devices, still consume energy by the semiconductor components residing in control circuits. DOE (DOE 2012a) presented the efficiency data of PWM VFDs with rated load from 5 to 200 HP provided by one VFD manufacturer. According to these data, the VFD efficiency is very high under the full load, varying from 95% to 97%, and slightly decreases as the load decreases. Currently, VFD energy losses are considered minimal, between 3% and 5% under the rated load.

Typically, the VFD output voltage is correlated to the VFD output frequency. Since the magnetic flux of motor iron cores is proportional to the ratio of VFD output voltage and frequency (V/f), excessive voltage would result in magnetic field saturation, and consequently an enormous magnetizing current and wholly unacceptable iron and copper losses (Hughes 2006). Therefore, a constant ratio of voltage to frequency was initially

applied to keep the constant magnetic flux and avoid the magnetic saturation for all applications (CAETI 2000, Hughes 2006, Eaton 2008).

Even though the constant voltage to frequency ratio does not account for motor energy performance, it actually works well for positive displacement compressors with constant torque. Constant torque demands constant rotor current with a constant voltage to frequency ratio. However, a constant voltage to frequency ratio typically provides motors with a higher amount of voltage than is required to control the attached reduced load for centrifugal machines, such as fans and pumps (Fehr 2011). Therefore, a ratio of voltage to the square of frequency is introduced for centrifugal machines.

Currently most VFDs in markets provide at least two preset voltage to frequency ratios (ABB 2011, Danfoss 2014, Eaton 2013, Schneider 2012 and Siemens 2013) recommended by Air-conditioning, heating and Refrigeration Institute (AHRI) Standard 1210 (2017). The ratio of voltage to frequency, called a liner ratio, is recommended for positive displacement compressors with constant torque loads while the ratio of voltage to frequency to the power of 2, called a squared ratio, is recommended for centrifugal fans, pumps and compressors with variable torque loads. It is clear that the linear ratio is derived from the consideration of the motor iron core saturation. However, it is undiscovered which principle is applied to obtain the squared ratio for centrifugal machines.

In addition to two preset voltage to frequency ratios, VFD manufacturers actually offer another choice to control the output voltage, which is often called energy optimization or flux optimization. Its purpose is to actively adjust the output voltage to maximize motor efficiency at the actual load.

1.2 Fault detection and diagnosis

Generally, the Fault Detection and Diagnosis (FDD) methods can be classified into three categories: the model-based, rules-based, and data-driven methods. The model-based FDD methods utilize physical or mathematical models which are developed based on understandings of the process concerned. Through comparing the real process outputs with the predicted ones from the models, the residues are obtained that can be used to detect and diagnose the faults. The rule-based methods employ expert knowledge or experiential rules. With a proper process of reasoning, a fault can be diagnosed through checking whether the abnormal symptoms match the expert knowledge or experiential rules. The data-driven FDD methods make use of historical operation data to capture the quantitative correlations among system variables (Du et al. 2014).

Different studies have been done on fault detection in fan and duct systems. Du et al. (2014) used a data-driven approach (artificial neural networks) to find the faults mostly related to supply air temperature control loop (related sensors and coil water valve) using the airflow, temperature and pressure as variables. (They used three flow sensors for outside air, return air and supply air). Liang et al. (2007) proposed a new method by combining the model-based FDD method and the Support Vector Machine (SVM) method. The faults which have been investigated were recirculation damper stuck, cooling coil fouling or blockage and supply fan speed decreasing. Their measuring parameters were supply air temperature, mixed air temperature, outlet water temperature, valve control signal, supply air pressure and room pressure. Lauro et al. (2014) presented

a hybrid statistical, clustering and rule-based approach in order to diagnostic abnormal electric consumptions of fan coils caused by improper use by the employees. Fan coil electric maximum power consumption of the building second floor was analyzed and considered in this experimentation with a 10 minutes time step. Furthermore, people presence and time of the day were recorded with a 10 minutes time step. Wang et al. (2004) detected air handling unit (AHU) sensor faults using the Q-statistic or squared prediction error (SPE). They are isolated using the SPE and Q-contribution plot supplemented by a few simple expert rules. The measuring parameters were temperature, humidity, flowrate and pressure. In another work (Wang et al. 2010), they did sensor FDD for HVAC systems including the cooling tower system, chiller system, secondary chilled water pump (SCHWP) system before heat exchangers, heat exchanger system and SCHWP system after heat exchangers. They used temperature and flowrate as controlling parameters. Norford et al. (2002) developed two methods for detecting and diagnosing faults in HVAC equipment. The one of the two fault FDD methods used first-principles-based models of system components. The data used by this approach were obtained from sensors typically installed for control purposes. The second method was based on semi-empirical correlations of submetered electrical power with flow rates or process control signals. The faults which they tried to detect were closed, stuck and leakage in recirculation damper, leaking cooling coil valve, reduced coil capacity, drifting fan pressure sensor, unstable supply fan controller and slipping supply fan belt. House et al. (1999) performed a study to demonstrate the application of several classification techniques to the problem of detecting and diagnosing faults in data generated by a variable-air-volume (VAV) AHU simulation model and to describe the strengths and

weaknesses of the techniques considered. Their measuring variables were temperature, pressure and airflow. In their study, they considered seven faults, stuck cooling coil valve, fouled cooling coil, leak in heating coil valve, stuck VAV box damper, fan belt slippage or decrease in the motor efficiency, failure of the return fan controller and failure of a linkage in the mixing box dampers. Carling (2001) compared three fault detection methods based on field data of an AHU. The three methods are: a qualitative method that compares controller outputs and model-based predictions, a rule-based method that examines measured temperatures and controller outputs and a model-based method that analyzes residuals based on steady-state models. He used temperature at different points, water side differential pressure over the coil, supply airflow, control signal to dampers and control signal to coil as measuring variables. He introduced the faults to the system as follows: The damper shafts were loosened from the actuators and turned to some position where they were mechanically locked. The coil valve position was manipulated by setting the control signal to a faulty value in manual mode. Installing an additional bypass pipe and valve, which allowed water to pass the valve despite the fact that it was closed, simulated the valve leakage. Lee et al. (2004) used general regression neural network models for FDD. Their measuring parameters were different temperatures, supply pressure, supply airflow, return airflow and humidity. The faults they were studied were most related to different sensors and control signals.

1.3 Virtual flow meters

Conventionally airflow and water flow rates are often measured by differential pressure meters, such as Pitot tubes, Orifice plates or Venturi meters, which normally require long, straight pipes or duct unobstructed by valves, dampers, bends and fittings

for accurate measurements (ASHRAE 2001). Wang (2014) gave an example that the total straight pipe length should be at least 3.89 m (13.8 ft) without any parts for a DN250 (NPS10) pipe. Unfortunately, these conditions are difficult to satisfy in actual systems and the accuracy of the physical flowmeter is in jeopardy. On the other hand, a component of HVAC systems may have a physical correlation of air or water flow rate with other measurable variables. For example, the pressure drop of a cooling coil is correlated to the water flow rate and the pressure drop of a control valve is correlated to the water flow rate as well as the valve position. Therefore, the flow rate can be virtually obtained by measuring other available variables. Zhao et al. (2015) developed a virtual water flow meter to determine the water flow rate in chillers using available chiller onboard measurements. Wang (2014) developed a method to determine the water flow rate through chillers by combining pipe resistance coefficients and online pressure difference. Song et al. (2013) developed a virtual water flow meter to determine the water flow rate through the cooling coil of AHUs based on pressure difference as well as control valve positions. Moreover, motor-driven fans and pumps are essential components installed in HVAC systems and share same governing laws. As discussed previously, since the fans and pumps have dynamic loads, VFDs are widely applied on the motors of fans and motors. The VFDs adjust the output frequency to proportionally reduce motor speed and consequently reduce motor mechanical load to pumps or fans. Meanwhile the VFDs also adjust the output voltage implicit to reduce motor electrical input power. The air or water flow rate through a fan or pump has a correlation with fan or pump head, shaft power, and speed. Therefore, a virtual flow meter can be developed on fans and pumps to determine the fan or pump flowrate by available fan or pump head,

shaft power, and speed (Wang et al. 2014). In general, the fan or pump head can be accurately measured by a differential pressure transducer, the fan or pump shaft power is easily obtained from the connected VFD, and the motor speed can be obtained from the VFD frequency command in building automation systems (BAS). Liu (2003) proposed the first fan airflow meter that determines fan airflow rate using measured fan head and speed associated with an in-situ fan head curve in 2003. Then a power-based fan airflow meter using measured fan power and speed was developed to eliminate the errors caused by the flat section of head curves in 2005 since the power curve is steep in the flow range where the head curve is flat in general (Wang et al. 2014). Liu (2006) demonstrated applications of both virtual fan and pump flow meters based on either head or shaft power. Besides the flat head and shaft power curves within a certain flow range, actual fan or pump speeds have to be applied to create actual correlations between head or shaft power and flow rate under actual speeds from the in-situ curve for both head-based and power-based virtual flow meters. Therefore, the fan or pump speed is a dominant variable that affects the accuracy of head-based and power-based virtual flow meters among all input variables. Unfortunately, the VFD frequency command does not always represent the motor speed, which is proportional to the fan or pump speed, especially in the low speed range. To avoid using inaccurate motor speeds, power-head-based fan and pump flow meters were developed. The power-head-based flow meters determines fan or pump flow rate based on measured fan/pump head and motor power as well as projected motor efficiency and fan/pump efficiency without using the motor speed. Motor efficiency is applied to calculate fan/pump shaft power from available motor power, which is read from the connected VFD. Meanwhile, fan/pump efficiency correlates fan/pump flow rate

to calculated shaft power and measured head, which is measured by a differential pressure transducer. Therefore, accurate motor and fan/pump efficiency calculation is essential to develop power-head-based virtual flow meters. The latest power-head-based fan flow meter was developed by Wang et al. (2014). Andiroglu et al. (2013) applied the same principle to develop and validate a virtual pump flow meter in 2013. Typically, the fan/pump efficiency curve normally is given as a function of flow rate under a design speed by manufacturers as same as the fan/pump head and shaft power curves. According to affinity laws, each point on the given efficiency curve under a design speed represents a series of equivalent points under different speeds, which have same efficiency as well as an identical ratio of fan/pump head to flow rate squared. Since the inaccurate fan/pump speed has to be avoided, the fan/pump efficiency was constructed as a function of the ratio of fan/pump head to flow rate squared through a calibration process in the latest power-head-based flow meters (Wang et al. 2014 and Andiroglu et al. 2013). Even though it is very common to assume constant motor efficiency for motor energy calculation (Montagud et al. 2014), accurate motor efficiency calculation is needed in virtual flow meter development for a better accuracy. The MotorMaster+ motor system management software developed by DOE's Industrial Technologies Program provides motor efficiency at different loads at the rated frequency for nearly 30,000 industrial electric motors (DOE 2008). In fact, not only motor power but also VFD frequency affects motor efficiency (Burt et al. 2008, Domijan et al. 1997 and Gao et al. 2001). Motor efficiency at variable frequencies can be accurately estimated using the motor equivalent circuit theory recommended by Institute of Electrical and Electronics Engineers (IEEE) (2004). The latest power-head-based flow meters applied this method

to calculate motor efficiency (Wang 2014 and Andiroglu 2013). The water flow determined by the developed virtual water flowmeter agrees well with the ultrasonic water flow meter measurement indicated by the coefficient of determination or R-squared of 0.97 and the standard deviation of 0.5 L/s (7 GPM) for instant measurement (Andiroglu 2013).

1.4 Problem statements

VFD manufacturers did not give any simulation or experimental supporting data for the preset voltage-frequency ratios. It is not clear whether the recommended ratios can achieve the highest motor efficiency or not and whether the recommended squared ratio works for all centrifugal fans and pumps with different pressure setpoints or not.

The model based approach usually have high computational cost which makes it unsuitable for using in BAS. The ruled based or hybrid approaches used in the literature whether did not use flow meters (which makes the FDD not accurate) or used physical flow meter.

In this study, the goal is to identify two major faults in HVAC systems, fan belt slippage and pressure set point override. Fan belt slippage fault is one the most common faults observed in AHUs which results in lower efficiency and increase in energy consumption of the fan. Pressure setpoint override fault significantly affects the control system resulting in poor indoor comfort and increase in energy consumption.

Two iterations in virtual flow calculation are barriers to implement the developed virtual flow meters in BAS. First, VFD voltage, frequency and motor slip are independent input variables to calculate motor power and efficiency using the motor equivalent circuit

method (IEEE 2004, Austin 2009 and Wildi 2002), therefore, motor efficiency has to be implicitly determined by motor power, VFD frequency and voltage by a numerical method. Second, since fan and pump efficiencies were calibrated as a function of the ratio of fan or pump head to flow rate squared, the unknown flow rate presents on both the side of the basic flow correlation equation. As a result, the flow rate has to be calculated from available pump/fan shaft power and head through another numerical process. Two numerical processes to calculate the motor efficiency and flow rate make it impossible to achieve the virtual flow rate calculation in BAS for current HVAC applications, which has less mathematic calculation capacity.

1.5 Objectives and approaches

The first purpose of this study is to investigate energy efficient voltage-frequency ratios of VFDs installed on the induction motors of fans and pumps using the motor equivalent circuit method. First, the motor load and speed ratio is defined or derived for each application, especially for the centrifugal fans and pumps with pressure control; then voltage is optimized at given frequency and its correlated motor speed and load; and finally the motor efficiency is simulated and compared under different voltages, including the optimal voltage as well as the voltages set by different preset ratios, the ratio of voltage to frequency to the power of 0.5, the ratio of voltage to frequency (to the power of 1), the ratio of voltage to frequency to the power of 1.5, and the ratio of voltage to frequency to the power of 2. Furthermore, it is disscussed how the design motor efficiency point affects the system operation and how the voltage to frequency ratios should change respectively. Some experiments have been done to investigate the

performance of preset voltage to frequency ratio (specially the flux optimization) and the theoretically developed ratios.

The second purpose of this study is to identify two major faults in HVAC systems, fan belt slippage and pressure set point override. To achieve this purpose, first experienxtial rules are developed based on underestanding of the system. Then, experimental data are collected and used to calibrate the experiential relationships. Fan belt slippage fault can be identified based on a relationship between fan power, head and speed (developed based on the affinity laws). Pressure setpoint override fault can be identified based on the fact that system pressure drop is proportional to flowrate to the power of 2. The main benefit of this approach is that there is no need of additional sensor installation on the system.

The last purpose of this study is to develop and validate a virtual head-power-based pump flow meter, which is easily implemented in BAS, by constructing an explicit water flow expression of available motor power and pump head to eliminate these two barriers, First the motor efficiency is regressed as an explicit function of motor power by consolidating dependent factors, including motor power, VFD frequency and voltage; then the pump efficiency is regressed as a function of pump shaft power and head without water flow rate; and finally experiments are conducted to develop, calibrate and validate a virtual pump water flow meter on a chilled water pump based on motor power and pump head along with regressed motor and pump efficiency functions. To further increase the accuracy of the virtual flow meter, the effects of harmanic distortion is investigated on the system and embedded into virtual flow meter development procedure.

As mentioned before, flow rate measurement are required for accurate FDD methods. Therefore, in this study, virtual flow meter development is going to be addressed first.

1.6 Dissertation outline

The literature about potential energy efficiency methods for VFD-motor-fan/pump systems is reviewed, then the problems are stated and the objectives and approaches are developed in chapter one. Two fundamentals, affinity laws and motor equivalent circuit methods are introduced in chapter two. In chapter three to five, the approaches to each problem (which are virtual flow meter, investigation of optimized VFD voltage to frequency ratio and fault dtection and diagnosis) are disscussed in detail and results for each part is represented. Finally the research outcomes are sumarized in the conclusion.

Chapter 2: Theory

Throughout this study, some theoretical concepts have been used to develop the energy efficiency methods for VFD-motor-fan/pump systems. The theories which are frquently used are affinity laws and motor equivalent circuit. In the following these theories are briefly introduced.

2.1 Affinity laws

The affinity laws for pumps/fans are used to express the relationship between variables involved in pump or fan performance (such as head, volumetric flow rate, shaft speed and power). The affinity laws apply to pumps, fans, and hydraulic turbines. In these rotary implements, the affinity laws apply both to centrifugal and axial flows.

The laws are derived using the Buckingham-π theorem. The affinity laws are useful as they allow prediction of the head discharge characteristic of a pump or fan from a known characteristic measured at a different speed or impeller diameter. The only requirement is that the two pumps or fans are dynamically similar, that is the ratios of the fluid forces are the same.

With impeller diameter (D) held constant:

Flow is proportional to shaft speed:

$$\frac{Q_1}{Q_2} = \left(\frac{\omega_1}{\omega_2}\right) \tag{2-1}$$

Pressure or Head is proportional to the square of shaft speed:

$$\frac{H_1}{H_2} = \left(\frac{\omega_1}{\omega_2}\right)^2 \tag{2-2}$$

Power is proportional to the cube of shaft speed:

$$\frac{W_1}{W_2} = \left(\frac{\omega_1}{\omega_2}\right)^3 \tag{2-3}$$

As it can be seen, affinity laws relate the volumetric flow rate (Q), the shaft rotational speed (ω), the pressure or head developed by the fan/pump (H) and the shaft power (W) together.

These laws assume that the pump/fan efficiency remains constant, which is rarely exactly true, but can be a good approximation when used over appropriate frequency or diameter ranges (i.e., a fan will not move anywhere near 1000 times as much air when spun at 1000 times its designed operating speed, but the air movement may be increased by 99% when the operating speed is only doubled). The exact relationship between speed, diameter, and efficiency depends on the particulars of the individual fan or pump design. Product testing or computational fluid dynamics become necessary if the range of acceptability is unknown, or if a high level of accuracy is required in the calculation. Interpolation from accurate data is also more accurate than the affinity laws.

2.2 Motor equivalent circuit method

In this section, motor equivalent cicuit as a method to theoretically estimate the motor efficiency is introduced. Based on IEEE Standard 112-2004, motor efficiency curves are normally given under rated frequency (60hz) and voltage (such as 480V). A typical motor efficiency curve can be presented in Figure 2-1.

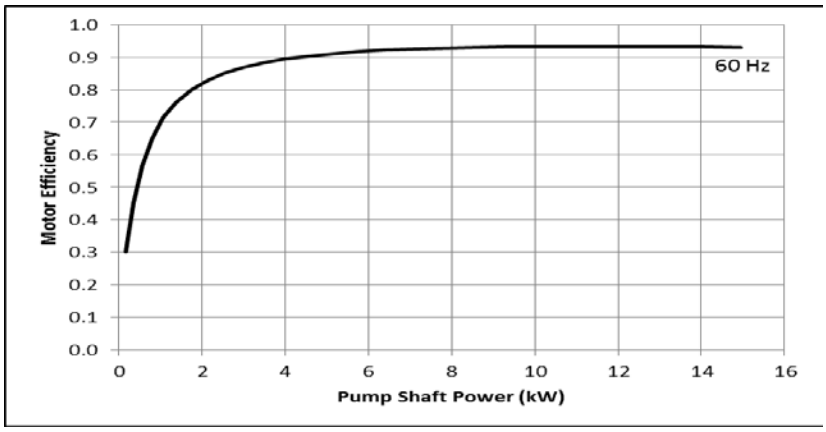

Figure 2-1 - Electrical motor efficiency curve.

As mentioned, VFDs reduce the frequency to reduce the motor speed. Therefore, the efficiency of the electrical motor needed to be known for different frequencies. To obtain accurate motor efficiency under variable frequencies, the equivalent circuit method proves effective. Hughes (2006) recommended that the equivalent circuit be applicable except under low frequencies, about 10 Hz for 60 Hz motors. A three-phase induction motor can be represented by three identical equivalent circuits. Figure 2-2 shows the schematics of an equivalent circuit with six circuit parameters, including stator winding resistance (R_1), rotor winding resistance (R_2), stator leakage reactance (X_1), rotor leakage reactance (X_2), magnetizing reactance (X_m), and core loss resistance (R_c).

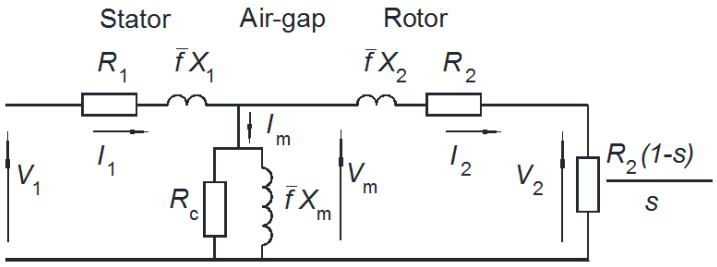

Figure 2-2 - Induction motor equivalent circuit.

Generally, the equivalent circuit method includes two steps: parameter identification and efficiency estimation. There are six circuit parameters which have to be identified to be able to use equivalent circuit method. In addition to the published nameplate data, which cannot indicate the motor performance over the full load range, the published motor efficiencies and power factors at the 25%, 50%, 75% and 100% rated loads are also adopted as the input data for obtaining the circuit parameters. This avoids the field test and also presents the motor performance over the full load range (Wang et al. 2013) .

In the circuit, the reactance is proportional to the VFD frequency while the resistance is independent of the VFD frequency. The relative VFD frequency ($\overline{f}$), the ratio of actual frequency to the rated frequency, is identical to the relative motor speed (ω) and is applied to calculate the reactance under varialbe frequency.

$$\overline{f} = \omega \tag{2-4}$$

Moreover, the load resistance is derived from the rotor resistance (R_2) using the motor slip (s).

$$R_{load} = R_2 \frac{1-s}{s} \tag{2-5}$$

It should be noticed that the voltage in the figure actually is the phase voltage rather than the line voltage, which is normally given for 3-phase induction motors. The stator or input current (I_1), the rotor or load current (I_2), the rotor or load voltage (V_2), and the magnetizing or air gap voltage (V_m) can be calculated based on the input voltage or VFD voltage (V_1) and the relative VFD frequency ($\overline{f}$) and the motor slip (s). The detailed calculation is listed in the Appendix.

Now the rotor mechanical output power (W_{rotor}) can be calcuated based on the load resistance.

$$W_{rotor} = 3I^2 R_{load} = 3I_2^2 R_2 \frac{1-s}{s} \tag{2-6}$$

The motor rotor mechanical output power (W_{rotor}) actually includes motor mechanical load (W) to the shaft and mechanical losses ($W_{F\&W}$). The mechanical losses include friction loss (W_F) due to bearing friction, and windage loss (W_W) due to air resistance, which is primarily caused by the cooling fan. Friction and windage losses under frequencies other than the rated frequency can be calculated from the rated friction and windage losses. The friction loss is proportional to the relative VFD frequency while the windage loss is proportional to the cube of the relative VFD frequency (Dey et al. 2008, Gieras et al. 1997).

$$W_{F\&W} = \overline{f} \cdot W_{F,d} + \overline{f}^3 \cdot W_{W,d} \tag{2-7}$$

Therefore, the motor mechanical load (W) can be calculated based on the calcuated rotor power and estiamted mechanical losses. In general, it can be expressed as a function of VFD voltage (V_1) , VFD frequency (f) and motor slip (s).

$$W = W_{rotor} - W_{F\&W} = f_W(V_1, f, s) \tag{2-8}$$

In return, the motor slip (s) is demanded by the motor load (W) as well as the VFD voltage (V_1) and frequency (f).

$$s = f_s(V_1, f, W) \tag{2-9}$$

The motor (input) power (W_{motor}) is balanced with the rotor mechanical output power (W_{rotor}) as well as the core loss on core loss resistance (R_c), the rotor loss on rotor winding resistance (R_2), and the stator loss on stator winding resistance (R_1).

Consequently the motor power is also a fucntion of the VFD voltage (V_1) and frequency (f) and the motor slip (s).

$$W_{motor} = \frac{3V_m^2}{R_c} + 3I_1^2 R_1 + 3I_2^2 R_2 + W_{rotor} = f_{Wmotor}(V_1, f, s) \tag{2-10}$$

For a given motor load, the motor efficiency represents the motor input power. The higher the motor efficiency is, the lower the motor power is.

$$\eta = \frac{W}{W_{motor}} = \frac{W}{f_{Wmotor}(V_1, f, s)} = f_\eta(V_1, f) \tag{2-11}$$

Using Equation (2-11), equivalent circuit method can be used to estimate motor efficiency under different frequencies. The results can be seen in Figure 2-3.

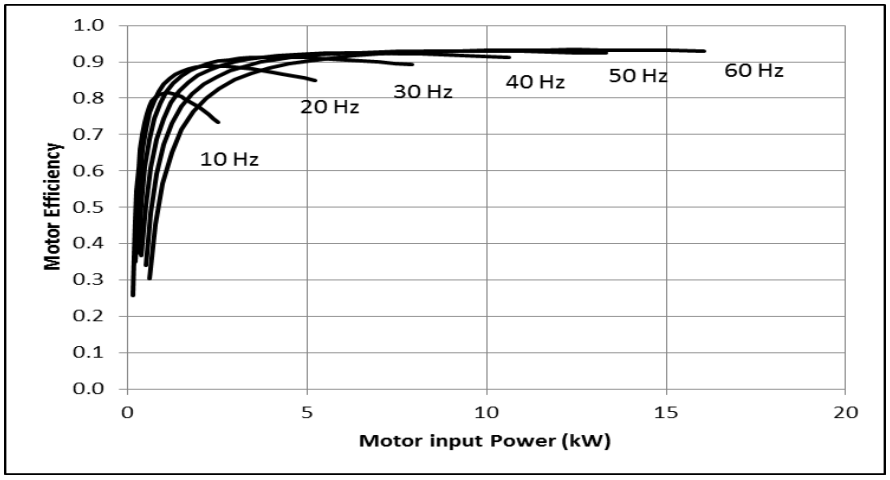

Figure 2-3 - Motor efficiency at different frequencies (calculated using motor equivalent circuit method).

Chapter 3: Virtual flow meter

As mentioned, VFDs are widely installed on the motor of pumps in HVAC systems to reduce pump shaft power by reducing VFD frequency and reducing motor power by reducing VFD voltage at partial flow rates. Figure 3-1 shows the configuration of a VFD-motor-pump system. The VFD receives the power at the rated frequency and voltage, and transforms it into the power at variable frequencies and voltages. The motor receives the power with variable frequencies and voltages from the VFD and drives the pump at variable speeds with reduced pump shaft power and motor power. The pump increases water pressure (head) and generates water flow driven by the shaft power from the motor.

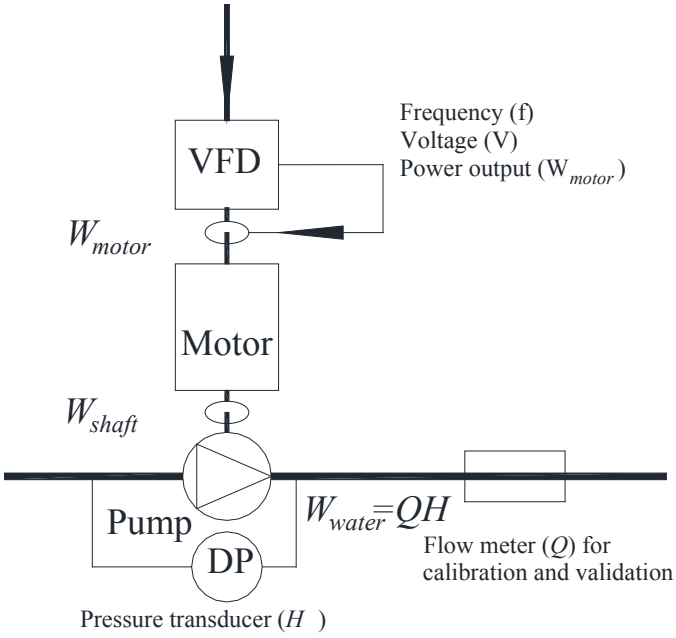

Figure 3-1 - A VFD-motor-pump system with available measurements.

As discussed previously, the pump head (H) can be easily and accurately measured by a differential pressure transducer (DP). Meanwhile, the motor power (W_{motor}) can be

easily obtained from the VFD control panel. Besides the motor input power, the VFD control panel also provides VFD frequency (f) and voltage (V). In other words, the VFD provides all necessary inputs for motor efficiency calculation. A portable ultrasonic water flow meter is also installed in the system in order to calibrate the virtual flow meter.

In order to develop a virtual pump water flow meter, the theoretical relation of the water flow rate through a pump with the available pump head and motor power will be explored. In this section, first, the basic relations as well as associated motor and pump efficiency functions in the latest power-head-based pump flow meter development (Andiroglu 2013) are reviewed, then two barriers for implementation in BAS are identified, and finally the solutions are proposed to eliminate these barriers.

3.1 Basic relation of pump water flow, head and motor power in the latest virtual meter

The mechanical work (W_{water}) imparted into water, which is the product of pump head (H) and water flow rate (Q), is determined by pump shaft power (W_{shaft}) along with the pump efficiency (η_{pump}).

$$W_{water} = H \cdot Q = W_{shaft} \cdot \eta_{pump} \tag{3-1}$$

Then the pump shaft power is determined by motor power (W_{motor}) along with the motor efficiency (η_{motor}).

$$W_{shaft} = W_{motor} \cdot \eta_{motor} \tag{3-2}$$

Therefore, the pump water flow rate (Q) can be obtained from the available pump head (H) and motor power (W_{motor}) with identified pump efficiency (η_{pump}) and motor efficiency (η_{motor}).

$$Q = \frac{W_{motor} \cdot \eta_{motor} \cdot \eta_{pump}}{H} \tag{3-3}$$

Equation (3-3) provides a basic relation for power-head-based virtual pump water flow meters. Since the pump head and motor power is measurable, the application of the relation relies on the pump and motor efficiency functions.

The affinity laws are applied to determine the pump efficiency independent with the motor speed. Each point on a pump efficiency curve under a design speed represents a series of equivalent points under different speeds, which have same efficiency and can be determined by a unique ratio of pump head to flow rate squared. Therefore, the speed independent pump efficiency curve is calibrated as a function of the ratio of pump head to flow rate squared.

$$\eta_{pump} = \frac{QH}{W_{shaft}} = \frac{QH}{W_{motor}\eta_{motor}} = \eta_{pump}(\frac{H}{Q^2}) \tag{3-4}$$

Substituting the implicit motor efficiency function, defined by Equation (3-1), and the pump efficiency function, defined by Equation (3-4), into the basic relation, defined by Equation (3-3), the virtual flow rate (Q) is an implicit function with respect of pump head (H) and motor power (W_{motor}) with another implicit function of the motor efficiency with respect of VFD voltage (V), frequency (f) and motor power (W_{motor}).

$$Q = \frac{W_{motor} \cdot \eta_{motor,imp}(V, f, W_{motor}) \cdot \eta_{pump}(\frac{H}{Q^2})}{H} \tag{3-5}$$

3.2 The barriers for implementation in BAS

In the latest power-head-based flow meter development as shown in Equation (3-5), the motor slip needs to be determined from available VFD voltage, frequency and motor

power through a numerical method based on the explicit function of the motor power with respect of the VFD voltage, frequency and motor slip, defined by Equation (3-2).

Moreover, the pump efficiency is structured as a function with respect of the ratio of pump head and flow rate squared, which results in unknown flow rate presenting in both the side of the basic relation, defined by Equation (3-5). Another numerical method has to be applied to determine the flow rate based on the available motor power and pump head besides a numerical method to determine the motor efficiency.

As a result, two numerical processes to determine motor efficiency and flow rate make it impossible to implement the developed virtual meter in the BAS.

3.3 Solution to eliminate numerical processes

The VFD usually has different settings for the voltage to frequency ratio, the ratio of VFD output voltage to VFD output frequency, even though a simple linear setting is to maintain a constant voltage to frequency ratio, which is always equal to the ratio of the rated voltage to the rated frequency. With any given voltage to frequency ratio setting, the VFD voltage is dependent on the VFD frequency. Moreover, with pump speed control in a chilled water system, the VFD frequency, which is proportional to the motor speed, is modulated to maintain a differential pressure in the chilled water system at its setpoint. As a result, the VFD frequency is correlated to the mechanical work (W_{water}) imparted into water and consequently to the motor power (W_{motor}). Therefore, the VFD frequency and voltage are dependent with the motor power. By consolidating these three dependent input variables, the motor efficiency is regressed as a function of the motor power only.

$$\eta_{motor} = \eta_{motor}(V(W_{motor}), f(W_{motor}), W_{motor}) = \eta_{motor}(W_{motor}) \qquad (3\text{-}6)$$

As a result, the motor efficiency is easily regressed as an explicit function with respect of the motor power for a given motor under a given voltage to frequency ratio setting and a given pump speed control sequence.

On the other hand, the affinity laws state that the pump flow rate is proportional to the pump speed, the pump head is proportional to the square of the pump speed and the power shaft power is proportional to the cube of the pump speed. As a result, a series of equivalent point can be defined by any two operating variables among the pump flow rate, head, shaft power and speed. Besides the ratio of pump head to water flow squared (H/Q^2), a series of equivalent points can be determined uniquely by the ratio of pump shaft power squared to pump head cubed ($W_{shaft}/H^{3/2}$).

Consequently, since the pump shaft power and head are always available, the pump efficiency can be regressed a function of the ratio of pump shaft power to pump head to the power of 3/2 rather than the ratio of pump head to water flow squared to avoid the unknown water flow rate in the pump efficiency calculation in Equation (3-4).

$$\eta_{pump} = \frac{QH}{W_{shaft}} = \eta_{pump}\left(\frac{W_{shaft}}{H^{3/2}}\right) \tag{3-7}$$

With newly developed pump and motor efficiency functions, defined by Equations (3-6) and (3-7), the pump water flow rate (Q) is correlated explicitly with the motor power (W_{motor}) and pump head (H).

$$Q = \frac{W_{motor} \cdot \eta_{motor}(W_{motor}) \cdot \eta_{pump}\left(\frac{W_{motor} \cdot \eta_{motor}(W_{motor})}{H^{3/2}}\right)}{H} \tag{3-8}$$

In order to apply the explicit flow relation, Equation (3-8), in BAS, the motor efficiency and pump efficiencies have to be calibrated. Figure 3-2 summarizes the calibration process marked by long dash arrows for motor efficiency and by short dash

arrows for pump efficiency and the meter development process marked with solid arrows for a proposed virtual pump water flow meter.

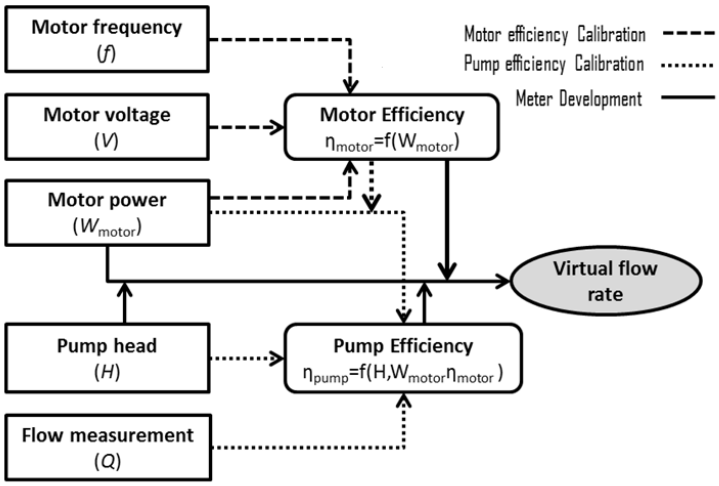

Figure 3-2 - Calibration and development of a virtual pump flow meter.

3.4 Experiments

Experiments were conducted on a VFD-motor-pump system in a building chilled water distribution system of the main library at University of Miami. The initial purpose of the experiments was to develop and validate a virtual pump flow meter using the principle proposed by Wang et al. (2014). Even though the results show that the virtually calculated water flow rate agrees well with the ultrasonic water flow meter measurement with the R-squared of 0.97 for instant measurement, two numerical processes were applied in the flow calculation. In this section, the flow rate is recalculated using the method proposed in the paper without any numerical process after the calibration.

The studied chilled water booster loop is a 0.2 m (or 8 inch) diameter main pipe fed by two pumps with alternating duty cycles and the VFD modulates the pump speed to maintain a building chilled water loop differential pressure setpoint. During the

experiments, the system was set to operate continuously using one pump only without duty cycling.

Real-time monitoring and data acquisition were established at the experiment site as shown in Figure 3-1. A four-channel data logger was used to record the motor power and VFD voltage from two VFD analog output channels and the VFD frequency from one VFD analog input channel. A differential pressure transducer was installed between the pump discharge and suction for pump head measurements. A conventional externally installed ultrasonic water flow meter was mounted on the chilled water pipe for the pump efficiency calibrations and virtual flow rate measurement validation.

Experiments were conducted from April 24th to May 17th 2013 with a sample interval of one minute. The data collected from April 24th to May 2nd were used to calibrate the motor and pump efficiencies to develop a virtual pump water flow meter, while the data from May 3rd to May 17th were used to validate the developed virtual pump water flow meter.

3.5 Motor efficiency calibration

A 15 kW (or 20 HP) 460 V three-phase induction motor with the rated frequency of 60 Hz and the rated voltage of 460V provides the shaft power to the pump. The circuit parameters are estimated based on the motor performance data provided by the motor manufacturer using the same method applied by Andiroglu et al. (2013) and listed in Table 3-1.

Table 3-1 - Calculated equivalent circuit parameters.

Parameter (ohm)	Value
Stator winding resistance	0.276
Stator leakage reactance	1.56
Magnetizing reactance	21.9
Core loss resistance	721
Rotor winding resistance	0.207
Rotor leakage reactance	1.05

With these six estimated circuit parameters, the motor efficiency (η_{motor}) is simulated using VFD voltage (V), frequency (f) and motor power (W_{motor}) using the motor equivalent circuit method.

Figure 3-3 shows the motor efficiency-power curves under six different motor frequencies with the constant voltage to frequency ratio. It is obvious that the motor efficiency is impacted by both the motor power and VFD frequency.

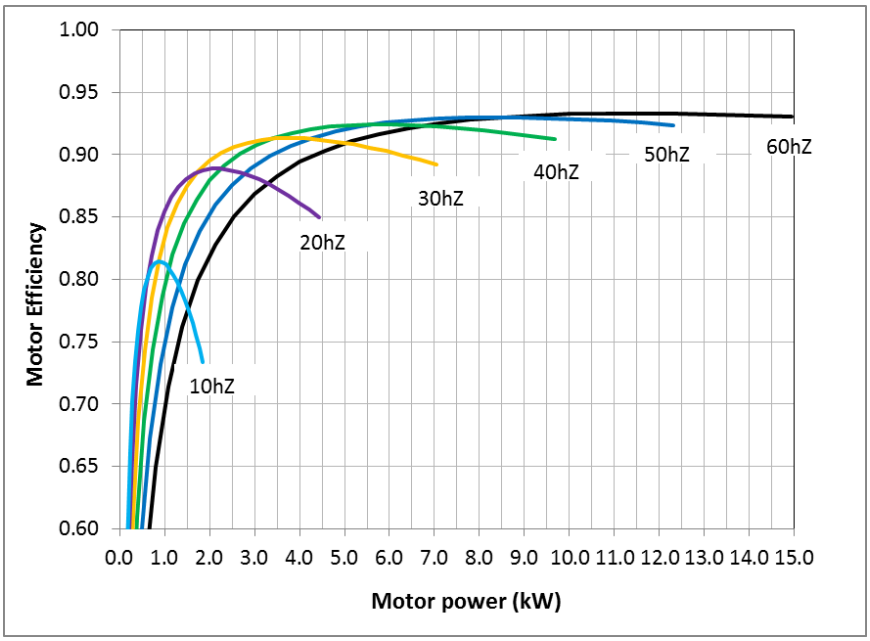

Figure 3-3 - Motor efficiency under different motor power and VFD frequency.

As discussed previously, the motor voltage and VFD frequency may be dependent with the motor power based on the voltage to frequency ratio setting in the VFD and the pump speed control sequence in BAS. Therefore, the dependency of the VFD voltage and frequency with the motor power need to be evaluated. The ratio of the VFD voltage and frequency in the VFD remained the initial linear setting and the system was operated under routine control sequences during the experiments.

Figure 3-4 shows the correlation between the motor voltage and power while

Figure 3-5 shows the correlation between the relative VFD frequency and motor power. The R-squared is 0.995 between the regressed and actual motor voltage and is 0.995 between the regressed and actual VFD frequency. Therefore, the VFD frequency and voltage are approximately dependent with the motor power, and the motor power is treated as an independent variable to determine the motor efficiency. Then the motor

efficiency is calculated based on the actual VFD frequency, voltage and motor power using the equivalent circuit method with Equation (3-6).

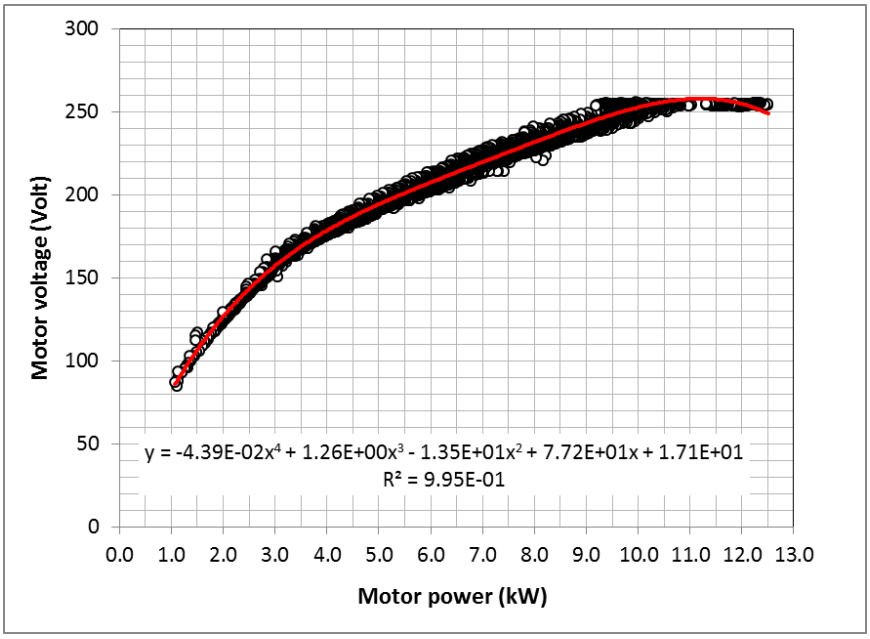

Figure 3-4 - Correlation between motor voltage and power.

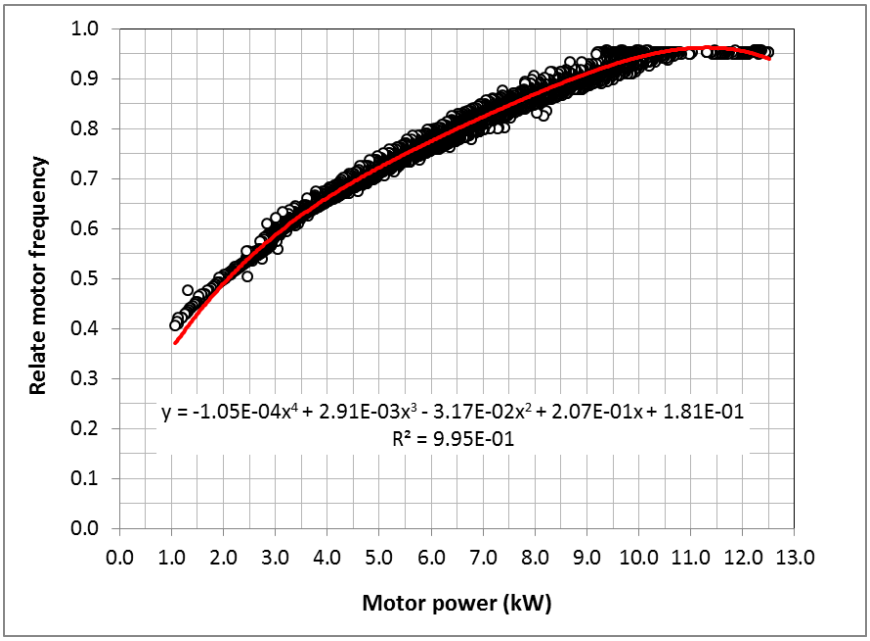

Figure 3-5 - Correlation between VFD frequency and motor power.

Figure 3-6 shows the motor efficiency versus motor power relation as well as the motor efficiency under different VFD frequency with a constant voltage to frequency ratio. It is obvious that the actual motor efficiency is actually the high efficiency bound for all VFD frequencies under the given motor power.

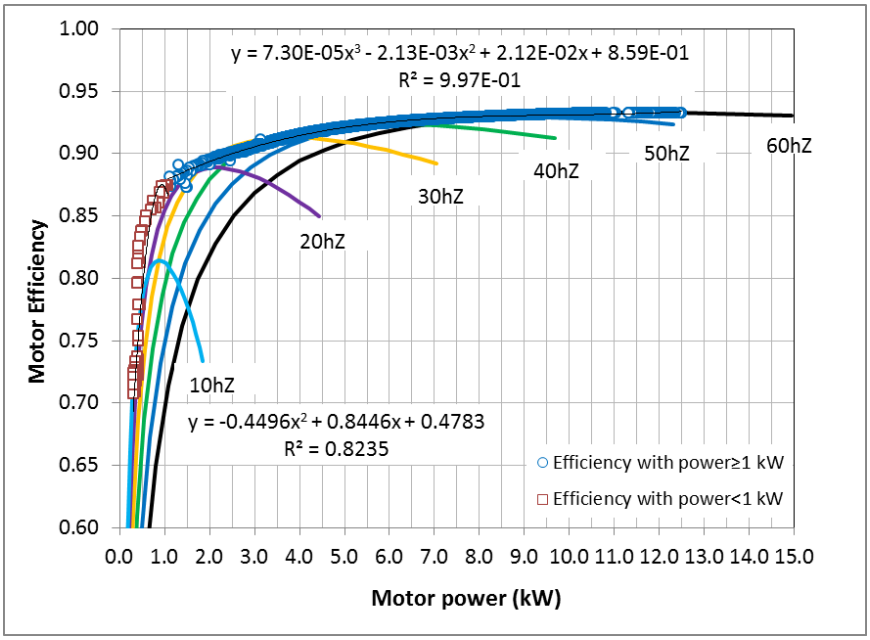

Figure 3-6 - Motor efficiency versus motor input power.

Figure 3-6 reveals that the motor efficiency slightly varies from 0.93 to 0.88 when the motor power varies from 12.5 kW to 1 kw but significantly drops from 0.88 to 0.70 when the motor power decreases from 1 kW to 0.3 kW. The relation between motor efficiency and power defined by Equation (3-6) is regressed as polynomials in two different motor power ranges.

$$\eta_{motor} = \begin{cases} 0.0000730W_{motor}^3 - 0.00213W_{motor}^2 + 0.0212W_{motor} + 0.859 & if W_{motor} \geq 1kW \\ -0.4496W_{motor}^2 + 0.8446W + 0.4783 & if W_{motor} < 1kW \end{cases} \quad (3\text{-}9)$$

3.6 Pump efficiency calibration

In this section, first it is explained why calibration is necessary for pump efficiency curves; then the pump efficiency calibration process is demonstrated. For experiment, the pump design water flow rate is 37.9 L/s (or 600 GPM), the design pump head is 239 kPa (or 80 ft of water) and the design pump shaft power is 12.1 kW (or 16.2 hp) at the full speed.

Pump efficiency curves can be developed using manufacturer's data but our experiments shows that there is a noticeable difference between manufacturer and experimental curves. The comparison between the pump efficency curves developed using manufacturer's data and experimental data are represented in Figure 3-7. It can be observed that in the most part of the pump operating range the efficiency difference is significant.

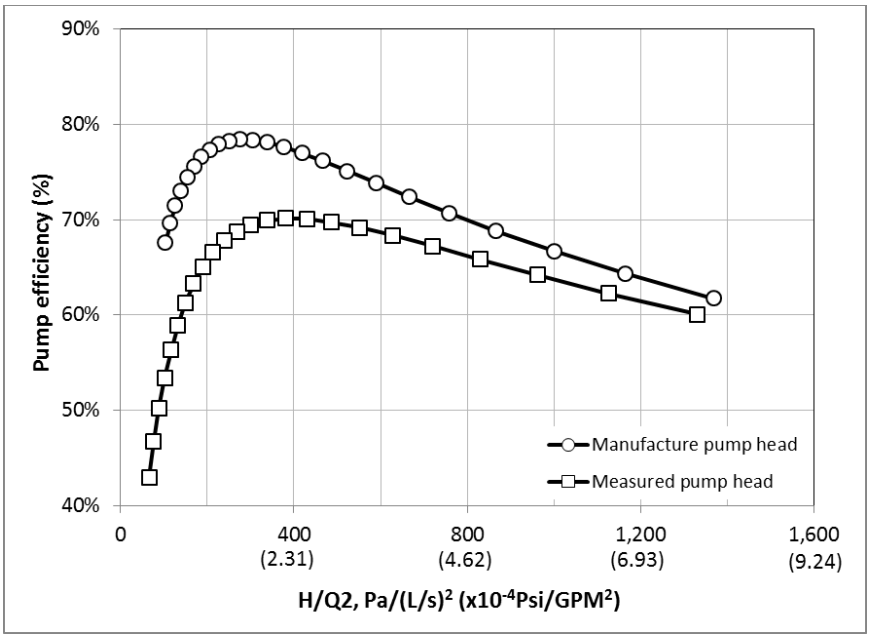

Figure 3-7 - Pump efficiency curves associated with measured and manufacturer pump head.

Equation (3-7) is applied to calibrate the correlation between the pump efficiency and the ratio of pump shaft power to pump head to the power of 3/2 based on the measured pump head and water flow rate, and motor power and efficiency.

Figure 3-8 shows the pump efficiency versus the ratio of the pump shaft power to the pump head to the power of 3/2 (new method) and Figure 3-9 shows the pump efficiency versus the ratio of pump head to flow rate squared (old method) for comparison.

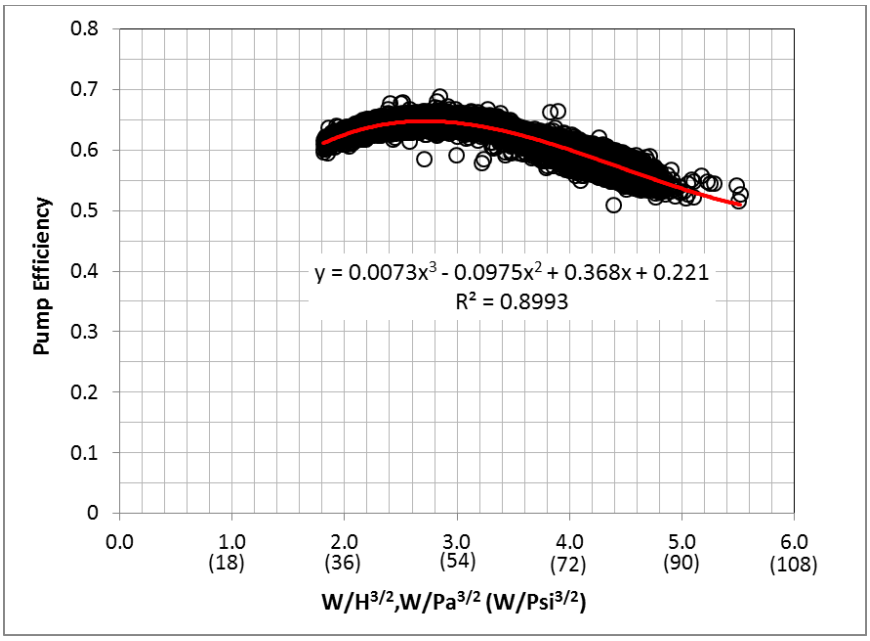

Figure 3-8 - Pump efficiency curve a s a function of pump shaft power to the pump head to the power of 3/2.

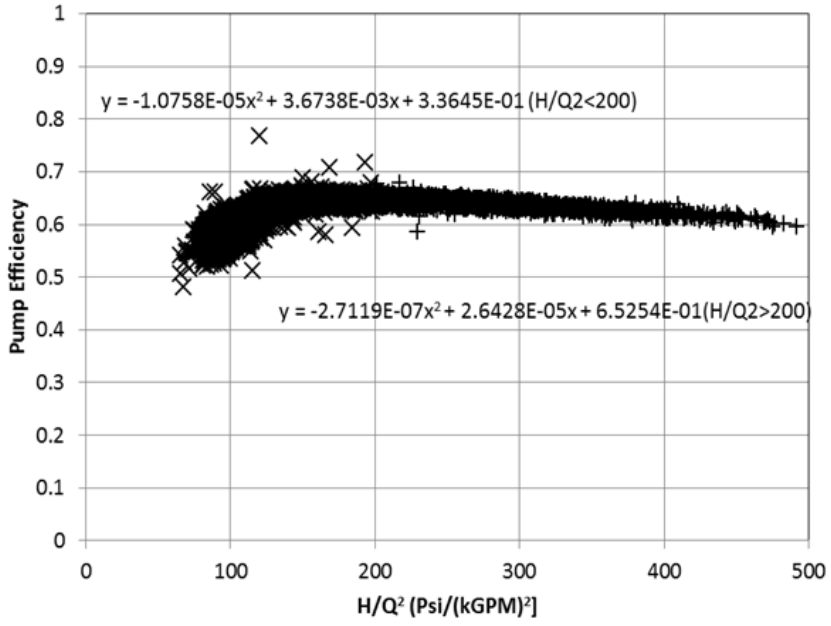

Figure 3-9 - Pump efficiency curve a s a function of pump head to flow rate squared.

The pump efficiency curve in Figure 3-8 is regressed with a third order polynomial of the ratio of the pump shaft power to the pump head to the power of 3/2.

$$\eta_{pump} = 0.0073\left(\frac{W_{shaft}}{H^{3/2}}\right)^3 - 0.0975\left(\frac{W_{shaft}}{H^{3/2}}\right)^2 + 0.368\left(\frac{W_{shaft}}{H^{3/2}}\right) + 0.221 \quad (3\text{-}10)$$

3.7 Validation

With calibrated motor efficiency, defined by Equation (3-9) and calibrated pump efficinecy, defined by Equation (3-10), the water flow rate through the pump is calculated from the available pump head and motor power using Equation (3-8). Since Equation (3-8) is an explicit water flow rate expression of the pump head and motor power, the developed virtual pump flow meter can easily implemented in BAS.

The data during the two-week validation period included 19,500 samples with a one-minute sample interval.

Figure 3-10 shows the motor power obtained from the VFD control panel, the moter efficiency calcuated based on the motor power using Equation (3-9) and the pump shaft power calcuated based on the measured motor power and calculated motor efficiency over a 6-hour period.

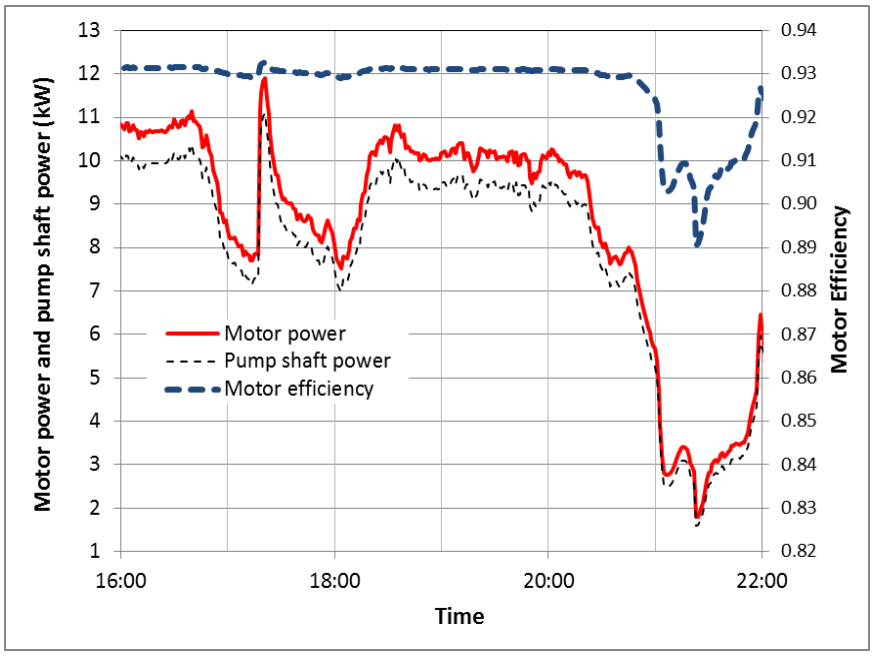

Figure 3-10 - Motor power, motor efficiency and pump shaft power over a 6-hour period.

Figure 3-11 shows the pump head measured by the pressure differential transducer, and pump efficiency calcuated from the raito of the calculated pump shaft power to the measured pump head to the power of 3/2 using Equation (3-10).

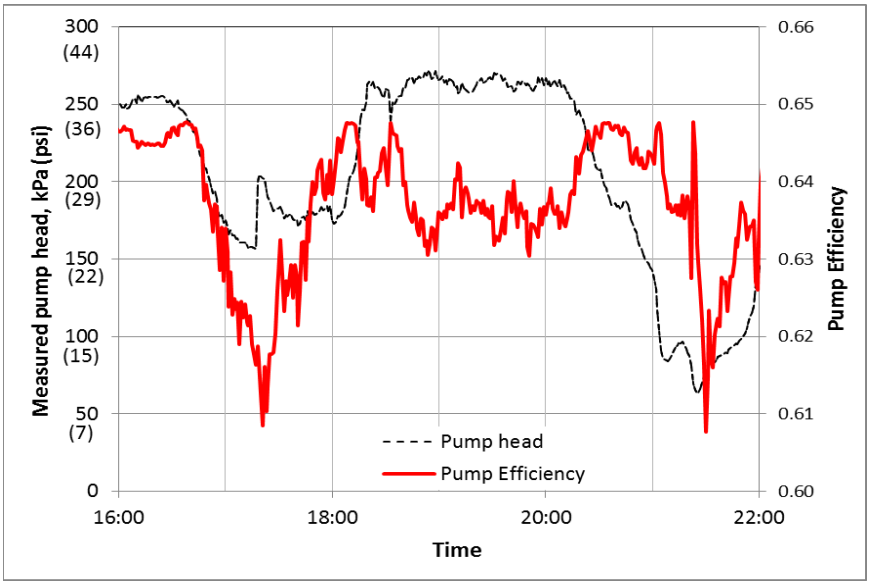

Figure 3-11 - Pump head and pump efficiency over a 6-hour period.

Finally the pump flow rate can be calcuated based on the measured pump head and calculated pump shaft power, shown in Figure 3-12.

Figure 3-12 compares the water flow rate measured by the ultrasonic water flow meter and the water flow rate calculated using Equation (3-8) over a same time period.

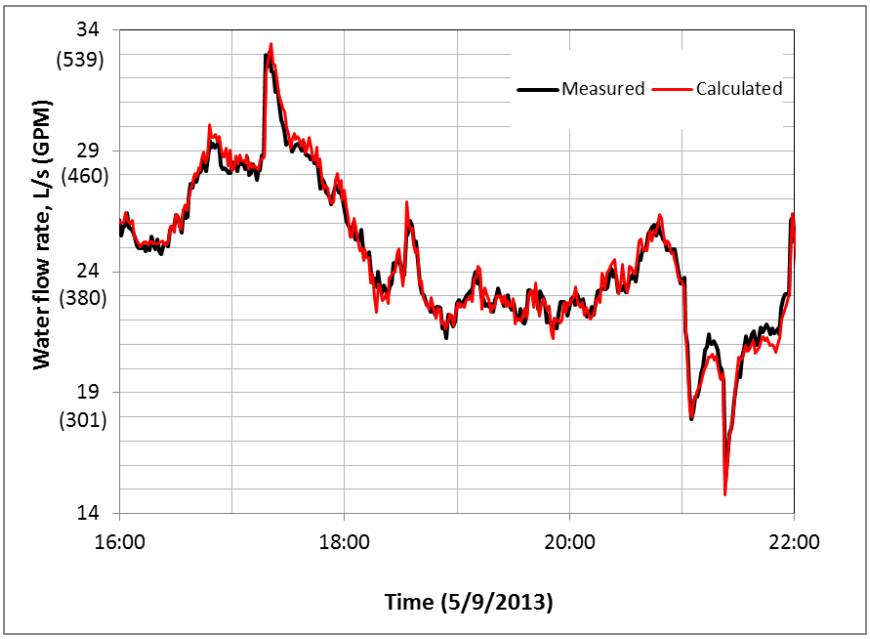

Figure 3-12 - Comparison of measured and calculated water flow rates over a 6-hour period.

Figure 3-13 compares measured and calcuated water flow and demonstates the flow error over the entire validation period from May 3rd to May 17th, 2013. The standard deviation for the entire validation period is 0.5 L/s (7 GPM) and the R-squared is 0.93 for the developed virtual pump flow meter. The results using the old method is represented in Figure 3-14. As it can be seen for the old method the R-squared is 0.91 which lower than the new method, so new method can improve the virtual flow meter accuracy.

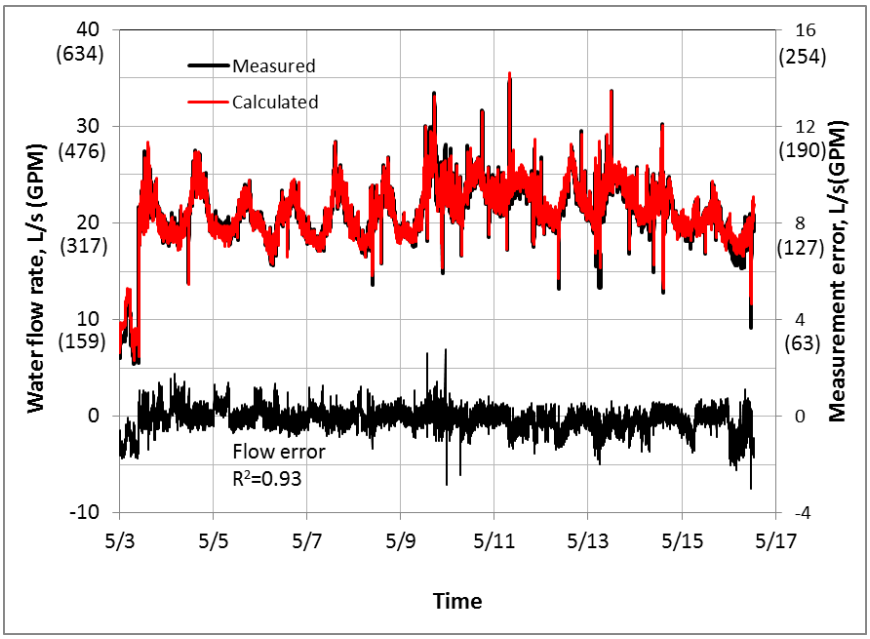

Figure 3-13 - Measurement errors over the entire validation period (new method).

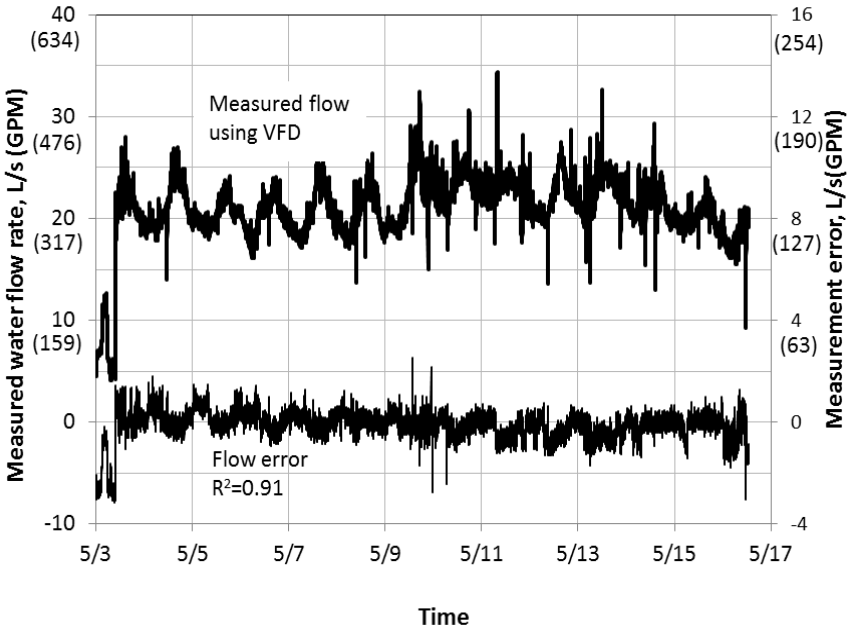

Figure 3-14 - Measurement errors over the entire validation period (old method).

Figure 3-15 presents the level of agreement between the water flow rates measured by the installed ultrasonic flow meter and the water flow rates calcuated by the devleoped virtual water flow meter. The experimental results show that the water flow measurements by the developed virtual flow meters agrees well with the physical water flow meter with the coefficient of determination or R-squared of 0.97, which is the same as the value obtained by Andiroglu et al. (2013) using two numercial processes.

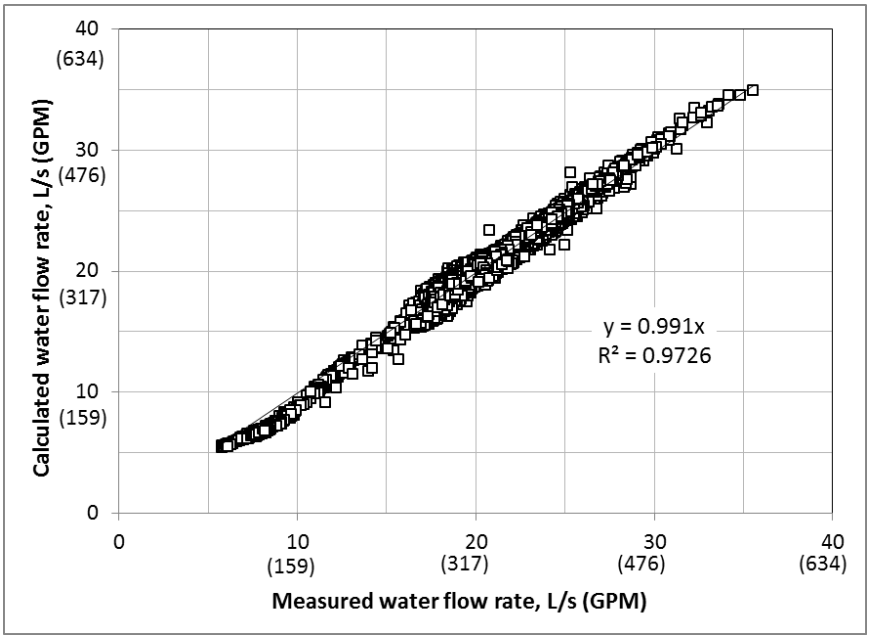

Figure 3-15 - Virtual water flow rate versus measured water flow rate.

3.8 Accuracy improvement

After implementation of the virtual flow meter in the system (which was part of the project sponsored by Department of Defense), it is observed when the supply fan operates at low speeds (which is associated with low motor frequency) the accuracy of virtual flow meter degrades. To solve this issue, an accuracy improving strategy is developed.

As mentioned, THD (total harmonic distortion) degrades the efficiency of electrical motor and THD generated by VFD can be regressed as the function of frequency. Therefore, to observe the effect of THD, motor efficiency can be developed as the function of frequency.

Experiments were performed to show the effect of THD on motor efficiency on a cooling tower fan (experimental setup is discussed in chapter 4.3). the results are represented in Figure 3-16, as it can be seen motor efficiency degradation with THD can be regressed as the function of frequency.

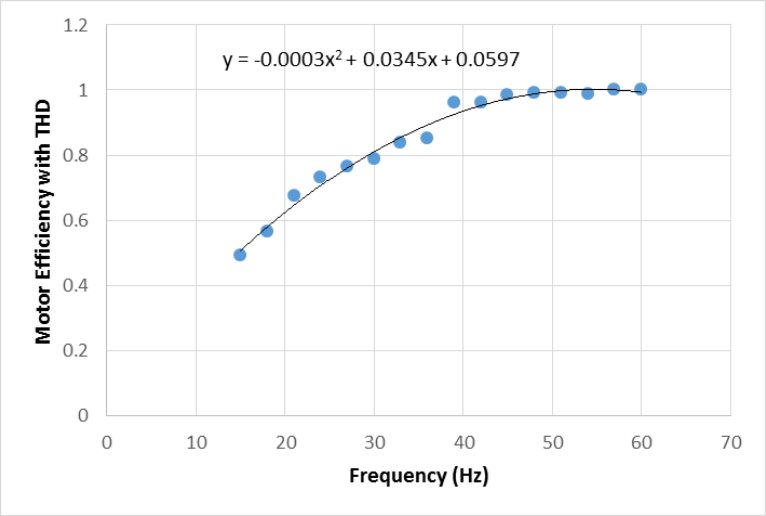

Figure 3-16 - Motor efficiency degradation (caused by THD) as the function of frequency.

In practice, since it is not feasible to use power meter in the system, the motor efficiency is developed as follows:

$$\eta_{motor} = \frac{Q_{calculated}}{Q_{measured}} \tag{3-11}$$

where $Q_{calculated}$ is the calculated flow rate before accuracy improvement and $Q_{measured}$ is the measured flow rate. The calculated motor efficiency from Equation (3-11) can be

used in Equation (3-3) to calculate the flow rate. In the following, the process of virtual flow meter accuracy improvement is demonstrated.

Figure 3-17 shows the efficiency versus the ratio of power to head to the power of 1.5. the red oval shows the regions were the efficiency degradation happens. For the fan efficiency calibration, the degraded efficiency data are removed (Figure 3-18).

Using Equation (3-11), motor efficiency effected by THD can be calculated and regressed as the function of frequency (Figure 3-19). As it can be seen, the motor efficiency degrades as the frequency gets lower.

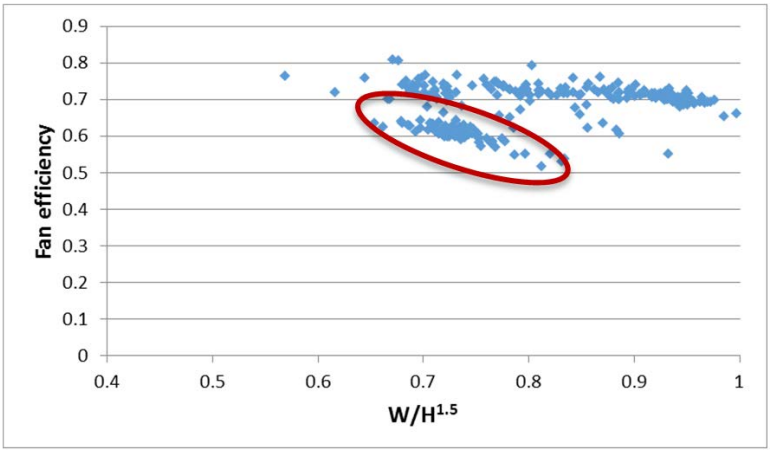

Figure 3-17 - Fan efficiency versus the ratio of power to head to the power of 1.5 (the red oval shows the fan efficiency degradation).

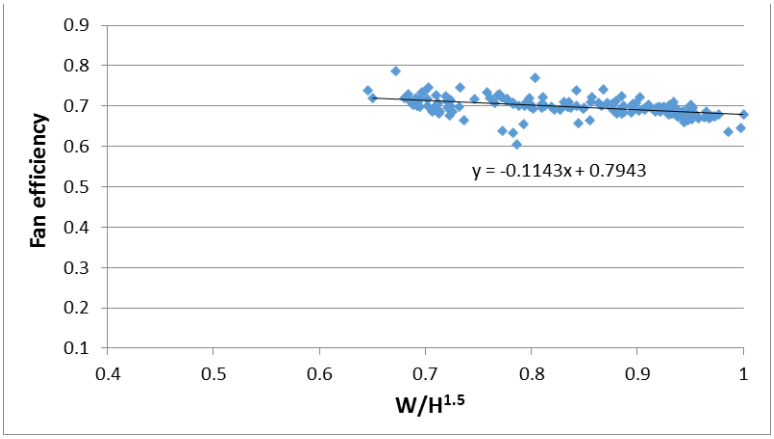

Figure 3-18 - Fan efficiency versus the ratio of power to head to the power of 1.5 (the data respective to fan efficiency degradation has been removed).

Now, using Equation (3-3), flow rate can be calculated. The results are represented in Figure 3-20. As it can be seen, in the low flow rate region, the measurement accuracy is significantly improved.

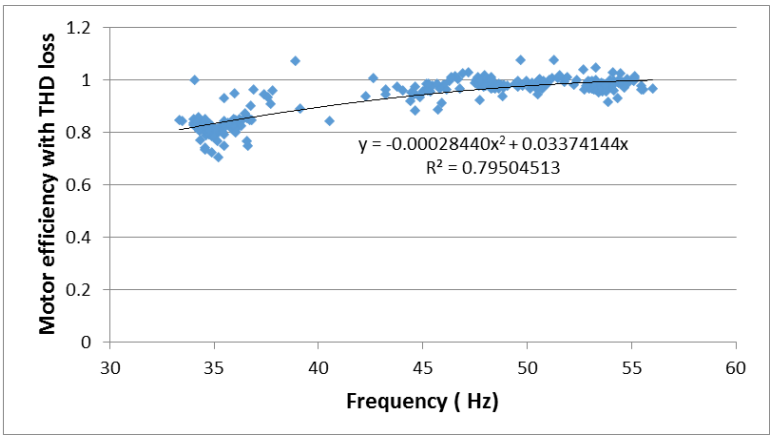

Figure 3-19 - Motor efficiency as a function of frequency.

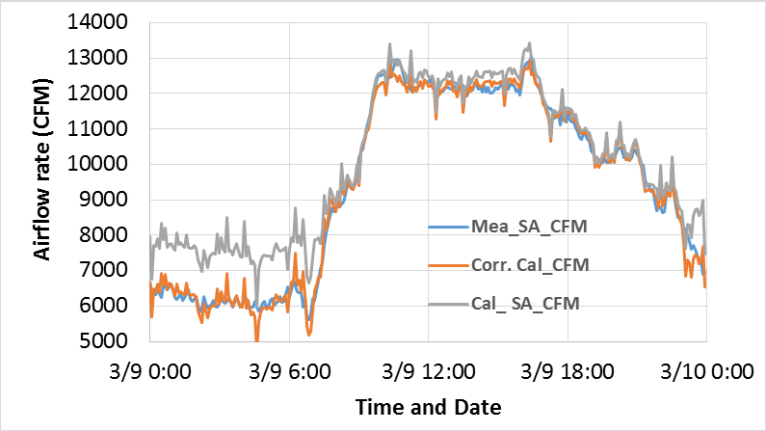

Figure 3-20 - Accuracy improvement of virtual flow meter (Blue line is the measured flow rate, the grey line is the calculated flow rate before accuracy improvement and the orange line is the calculated flow rate after accuracy improvement).

Chapter 4: Investigation of optimal VFD voltage to frequency ratio

Besides the ideal cubic and linear relations between the motor load and speed, the actual correlations for centrifugal fans and pumps with pressure control are indistinct and are explored first. Then the equivalent circuit method of induction motors is introduced in order to evaluate the motor efficiency at different VFD output voltage and frequency and motor load; and to consequently search the optimal voltage at given VFD frequency and its correlated motor speed and load. Finally, in order to evaluate the motor efficiency with preset voltage-frequency ratios, the voltage set by four voltage-frequency ratios is defined.

4.1 Simulation approach

4.1.1 Relation of motor load and speed

As discussed previously, the centrifugal fans and pumps without pressure control, such as the fans in cooling towers and condensers, and the primary pumps in decoupled hot water and chilled water systems, follow the ideal cubic relation between the motor load and speed. The motor load (W) is proportional to the cube of the relative motor speed (ω), a ratio of actual speed to the design speed.

$$W = W_d \cdot \omega^3 \tag{4-1}$$

Moreover, the displacement compressors observe the ideal linear relation between the motor load and speed with constant torque. The motor load (W) is proportional to the relative motor speed (ω).

$$W = W_d \cdot \omega \tag{4-2}$$

On the other hand, for the centrifugal fans and pumps with pressure control, such as the supply fans in VAV AHUs and the secondary pumps in decoupled hot water and chilled water systems, the fan and pump shaft power or motor load has to be determined by fan or pump performance curves as well as the system control curve with a given pressure setpoint.

The fan or pump performance curves are presented by the fan or pump head (H) curve and shaft power (W) curve at a design speed, which can be regressed as functions of flow rate (Q).

$$H = a_H Q^3 + b_H Q^2 + c_H Q + d_H \tag{4-3}$$

$$W = a_W Q^3 + b_W Q^2 + c_W Q + d_W \tag{4-4}$$

The fan or pump head and shaft power curves under a partial speed can be deduced using the affinity laws.

$$\frac{H}{\omega^2} = a_H \left(\frac{Q}{\omega}\right)^3 + b_H \left(\frac{Q}{\omega}\right)^2 + c_H \left(\frac{Q}{\omega}\right) + d_H \tag{4-5}$$

$$\frac{W}{\omega^3} = a_W \left(\frac{Q}{\omega}\right)^3 + b_W \left(\frac{Q}{\omega}\right)^2 + c_W \left(\frac{Q}{\omega}\right) + d_W \tag{4-6}$$

The system control curve is determined by the pressure setpoint (H_{sp}), which is measured by a pressure differential sensor and is maintained by modulating VFD output frequency. The system pressure drop includes the pressure drop upstream the pressure sensor, which is approximately proportional to the flow rate squared, and the pressure drop downstream the pressure sensor, which is approximately constant and equal to the pressure setpoint. The fan or pump head will overcome the system pressure drop.

$$H = H_{sp} + (H_d - H_{sp}) \cdot \left(\frac{Q}{Q_d}\right)^2 \tag{4-7}$$

Under a given flow rate, the motor speed can be determined by Equations (4-6) and (4-7). Then the shaft power or motor load can be determined by the given flow rate and calculated motor speed using Equation (4-6). Finally the motor load and speed can be correlated by the given flow rate. In general, the motor load can be expressed as a function of the motor speed.

$$W = W_d \cdot f_{W-\omega}(\omega) \tag{4-8}$$

According to Equations (4-5) to (4-7), with zero pressure setpoint, the correlation between the motor load and speed exactly follows the ideal cubic relation. Therefore the centrifugal fans and pumps with zero pressure setpoint also represent the centrifugal fans and pumps without pressure control with the ideal cubic relation.

4.1.2 Voltage set by fixed preset ratios

Since the easiest way to control the VFD voltage is to use fixed voltage-frequrency ratios, such as the ratio of voltage to frequency to the power of 2 (the squared ratio) and the ratio of voltage to frequency (the linear ratio) currently recommended by VFD manufacturers, a total of four voltage-frequency ratios are investigated to evaluate energy efficient voltage in the paper. The actual VFD voltage is determined by the rated volage (V_d) and the relative VFD frequency ($\overline{f}$) based on different voltage to frequency ratios.

With the ratio of voltage to frequency to the power of 0.5 or the square roof of frequency

$$V_1 = V_d \cdot \overline{f}^{0.5} \tag{4-9}$$

With the ratio of voltage to frequency (to the power of 1) (the linear ratio)

$$V_1 = V_d \cdot \overline{f} \tag{4-10}$$

With the ratio of voltage to frequency to the power of 1.5

$$V_1 = V_d \cdot \overline{f}^{1.5} \tag{4-11}$$

With the ratio of voltage to frequency to the power of 2 or the square of frequency (the squared ratio)

$$V_1 = V_d \cdot \overline{f}^{2} \tag{4-12}$$

The motor efficiency under the preset VFD voltages defined by Equations (4-9) to (4-12) along with the optimal voltage is evaluated using Equation (4-8) in the next section.

4.1.3 Applications

A 15kW (20HP) induction motor is selected to investigate the motor efficiency at the optimal voltage and four preset voltages in different applications. The motor can be applied either on a centirfugal pump or fan without pressure control to form an ideal cubic motor load relation defined by Equation (4-1). Moreover, the motor also can be applied on a centirfugal pump or fan with pressure control with an indistinct motor load relation.

In this section, the indistinct motor load correlation for a centirfugal fan or pump with a pressure control is first identified based on the pump performance curves and system control curve. Then, the motor equivalent circuit is defined for the selected motor and is applied to search the optimal voltage for the identified and ideal motor load-speed correlations. Finally, the motor efficiency under the optimnal voltage and the voltages set by fixed voltage-frequency ratios is simulated and compared.

4.1.4 Pump performance curves

A centrifugal pump is selected based on the design flow of 37.9 L/s (or 600 GPM) and the design head of 269 kPa (or 90 ft of water). The pump head and power curves at the design speed of 1,750 rpm were obtained from the pump manufacturer catalog, shown in Figure 4-1. The design shaft power is 13.1 kW at the design conditions.

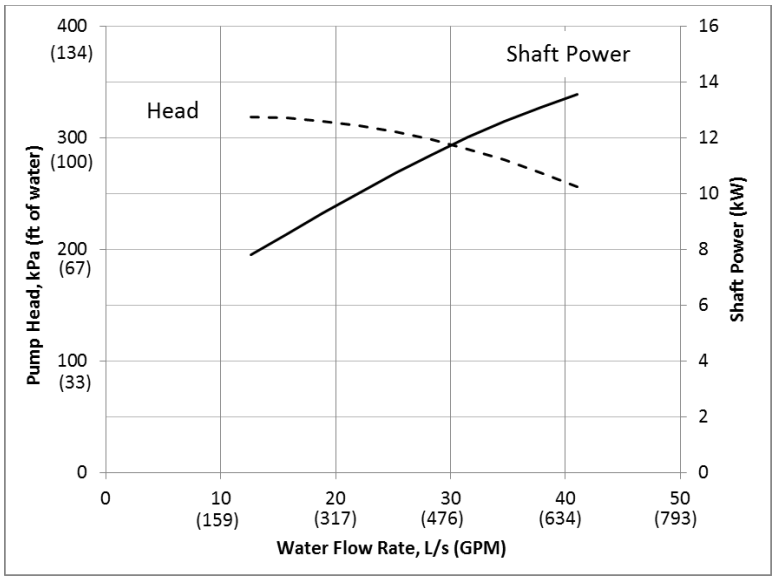

Figure 4-1 - Pump head and power curves at a design speed.

The pump head and power curves at the design speed can be expressed as polynomials with pump head in kPa, water flow in L/s and shaft power in kW.

$$H = 0.000074911Q^3 - 0.078241Q^2 + 1.8144Q + 308.31 \qquad (4\text{-}13)$$

$$W = -0.000037516Q^3 + 0.0010280Q^2 + 0.23533Q + 4.7501 \qquad (4\text{-}14)$$

4.1.5 System curve with different setpoints

The pressure setpoint is set at 0 kPa (0 ft of water), 67.5 kPa (22.5 ft of water) and 135 kPa (45ft of water) respectively to investigate the impact of different pressure setpionts on the motor load and speed relation. The pressure setpoitns are 0%, 25% and

50% of the design pump head. Figure 4-2 shows the system control curves with different pressure setpoints as well as the pump head curve at the design speed.

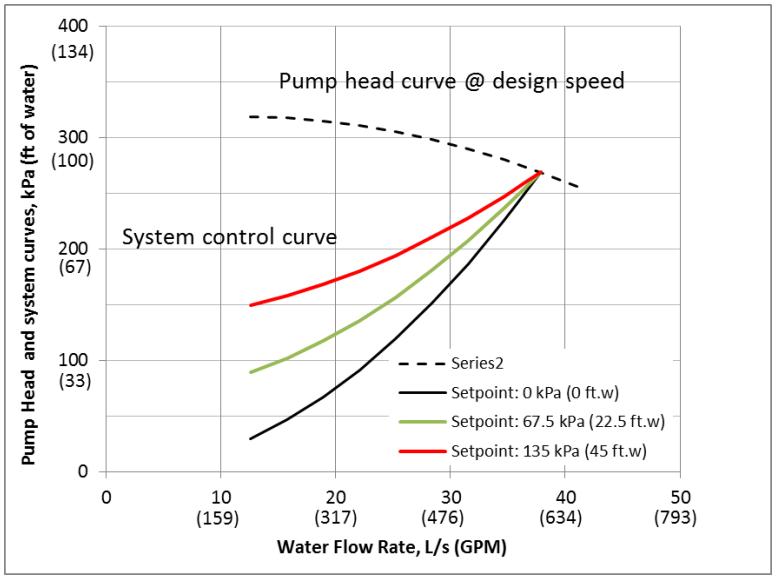

Figure 4-2 - System control curves with different setpoints.

4.1.6 Relations between the motor load and speed

As discussed previously, the relations for the centrifugal fans and pumps with pressure control depend on the pump curves and system control curve associated with the pressure setpoints. Under a given flow rate, the motor speed can be determined by combining Equations (4-6) and (4-8). Then the shaft power can be determined by the given flow rate and calculated motor speed using Equation (4-7). Figure 4-3 shows the calcuated shaft power (or motor load) and speed with three different pressure setpoints.

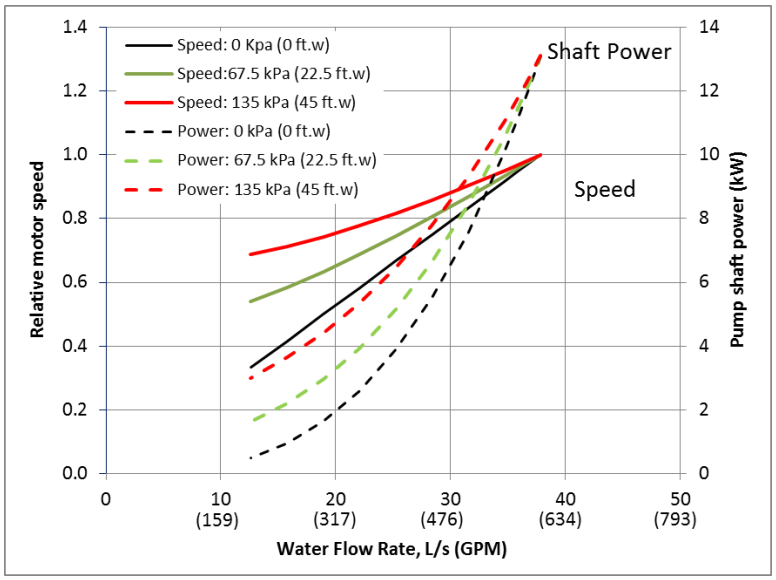

Figure 4-3 - Motor load and speed with different setpoints.

Finally the motor load and speed for the pumps with pressure control can be related through the the pump water flow. The relations are shown in Figure 4-4. It is obvious that the relation with zero pressure setpoint observes the ideal cubic relation. Meanwhile, the linear relation for displacement compressors with constant torque is also drawn in Figure 4-4.

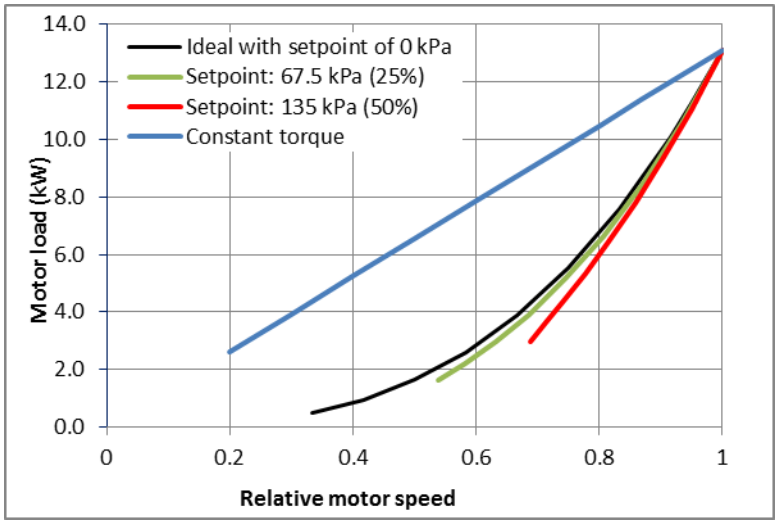

Figure 4-4 - Relation between motor load and speed.

Wang et al. (2015) defined a 15kW (20HP) induction motor with the rated line voltage of 460V and the rated frequency of 60 hz, which is selected in the paper. Its circuit parameters are listed in Table 4-1. It is also assumed that the mechanical losses are 10% of the total loss and the friction loss is identical to the windage loss under the rated power and frequency. The estimated circuit parameters and assumed mechanical losses are used to simulate the motor efficiency at different VFD frequency and voltage for four different applications defined in Figure 4-4.

Table 4-1 - Estimated equivalent circuit parameters.

Parameter	Value (ohm)
Stator winding resistance	0.276
Stator leakage reactance	1.56
Magnetizing reactance	21.9
Core loss resistance	722
Rotor winding resistance	0.207
Rotor leakage reactance	1.05

4.1.7 Optimal voltage

The optimal voltage is searched to achieve the highest motor efficiency for different relative motor speed or VFD frequency for four applications in Figure 4-4 using the motor efficiency function determined by Equation (4-8). Figure 4-5 shows the optimal

voltages for four applications as well as the voltages set by four fixed voltage-frequency ratios under different motor speed or VFD frequency.

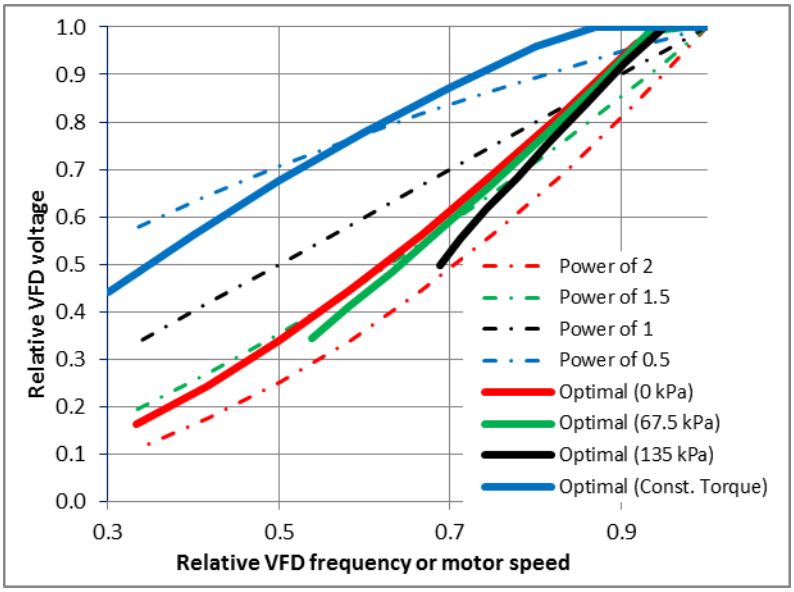

Figure 4-5 - Optimal voltages as well as voltages set by fixed frequency ratios.

The four optimal voltages include:

- Red solid line for the pump with pressure setpoint of 0% design pump head, which follows the ideal cubic motor load-speed relation
- Green solid line for the pump with pressure setpoint of 25% design pump head
- Black solid line for the pump with pressure setpoint of 50% design pump head
- Blue solid line for the idea linear load-speed relation with constant torque
- The four preset voltages, which are defined by Equations (4-9-4-12), include
- Red dash line for the ratio of voltage to frequency to the power of 2,
- Green dash line for the ratio of voltage to frequency to the power of 1.5
- Black dash line for the ratio of voltage to frequency (to the power of 1)

- Blue dash line for the ratio of voltage to frequency to the power of 0.5
- Several findings can be explored from Figure 4-5
- As the power of frequency increases from 0.5 to 2, the decreasing rate of a preset voltage will increases as the frequency decreases.
- The voltage set by the ratio of voltage to frequency to the power of 2 is not optimal for the centrifugal fans and pumps, even though with the purely cubic relation. Moreover, the voltage set by the ratio of voltage to frequency is not optimal for the displacement compressors with the ideal linear relation.
- The optimal voltage for the centrifugal fans and pumps with the pressure control depends on the pressure setpoint.
- The simulated optimal voltage remains at the rated voltage as the VFD frequency (or motor speed) just decreases from the design condition and then decreases as the VFD frequency (or motor speed) decreases after that.

4.1.8 Motor efficiency under different voltages

Now the motor efficiency under the optimal voltage and the voltages controlled by four preset ratios, presented in Figure 4-5, is simulated for four different applications, defined in Figure 4-4. Figure 4-6 to Figure 4-8 show the motor efficiency for the centrifugal pump with setpoint of 0 kPa (0 ft or water), 67.5 kPa (22.5 ft of water) and 135 kPa (45 ft of water) and Figure 4-9 shows the motor efficiency for constant torque application.

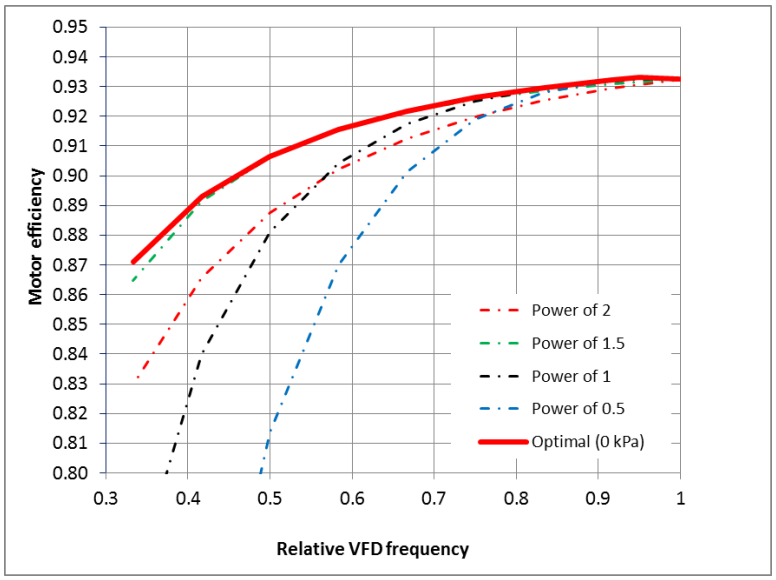

Figure 4-6 - Motor efficiency with optimal voltage and voltages by fixed preset ratios for Pump with setpoint of 0 kPa (0 ft of water).

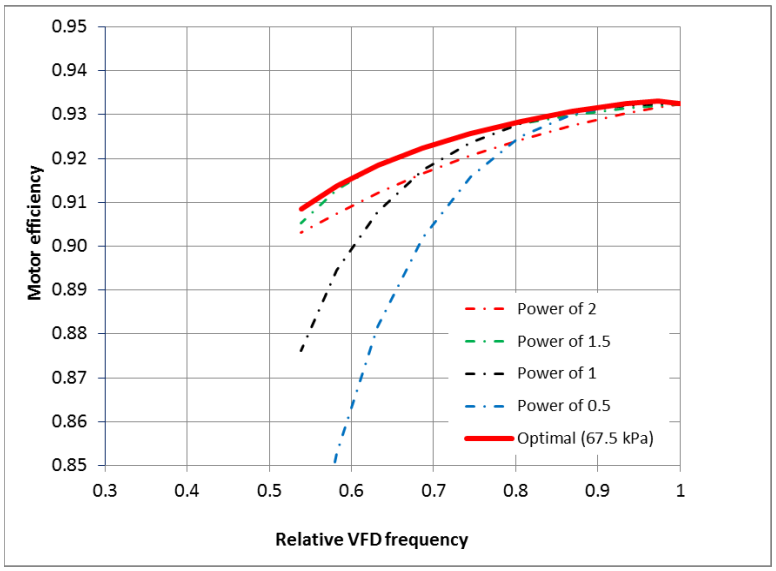

Figure 4-7 - Motor efficiency with optimal voltage and voltages by fixed preset ratios for Pump with setpoint of 67.5 kPa (22.5 ft of water).

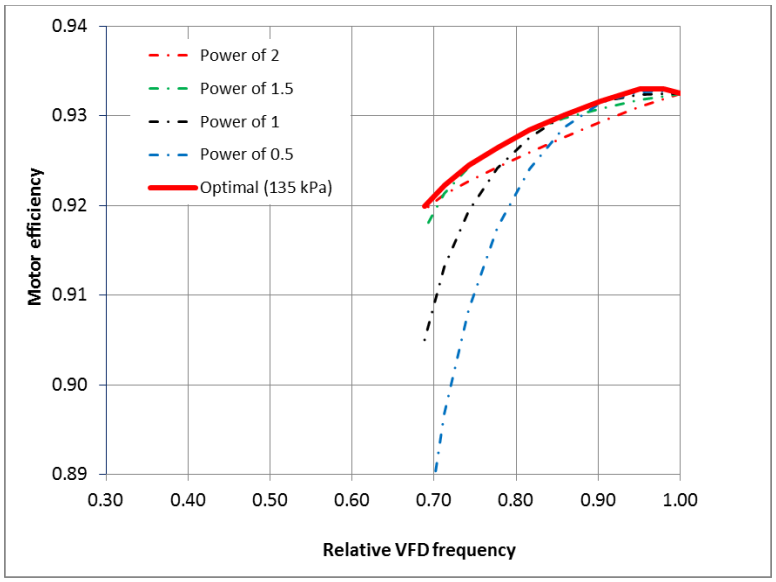

Figure 4-8 - Motor efficiency with optimal voltage and voltages by fixed preset ratios for Pump with setpoint of 135 kPa (45 ft of water).

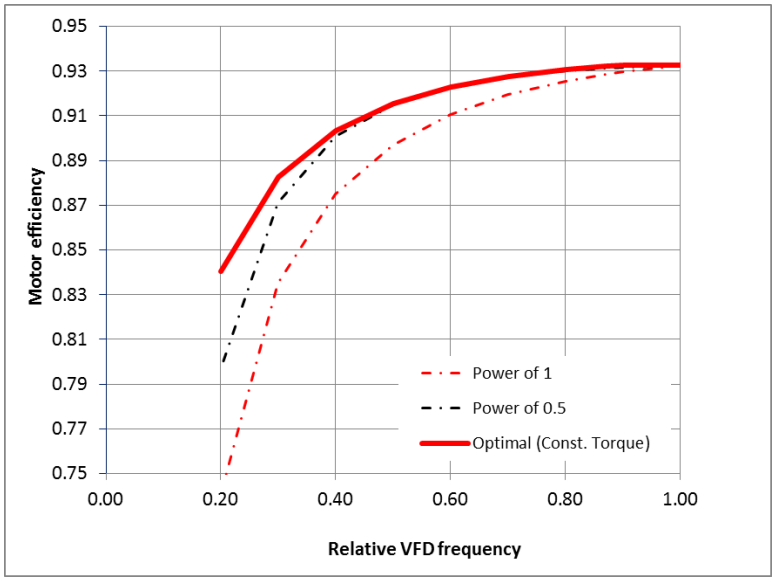

Figure 4-9 - Motor efficiency with optimal voltage and voltages by fixed preset ratios for Compressor with constant torque.

It is obvious that the optimal voltage can improve the motor efficiency over all VFD frequency ranges, for instant, by 3% at 40% of the full speed, over the voltages preset by

the recommended ratios by VFD manufacturers in both the ideal cubic and linear motor load-speed relation applications. It can also be seen that the voltage set by the ratio of voltage to frequency to the power of 1.5 is close to the optimal voltage for the applications with the ideal cubic motor load-speed relation and the voltage set by the ratio of voltage to frequency to the power of 0.5 is close to the optimal voltage for the ideal linear motor load-speed relation.

4.1.9 Discussions

Based on the motor equivalent circuit, shown in Figure 1, the VFD voltage, frequency and motor slip determine the motor performance parameters, such as motor load and power as well as efficiency. To explore the circuit in more detail, the motor load and power are approximately proportional to the VFD voltage squared because of minimal motor mechanical losses. Therefore, a normalized motor load ($\overline{W}$), the ratio of the motor load to the VFD output voltage squared, and the motor efficiency, the ratio of motor load to motor power, are independent with the VFD voltage.

Moreover, since the VFD frequency only affects the reactance, the normalized motor load and motor efficiency depends significantly on the motor slip and insignificantly on the VFD frequency.

$$\overline{W} = \frac{W}{V_1^2} \approx f_{\overline{W}}(s) \tag{4-15}$$

$$\eta = \frac{W}{W_{motor}} \approx f_{\eta}(s) \tag{4-16}$$

The normalized motor load and motor efficiency with two relative VFD frequency groups, 100% and 50%, are drawn versus the motor slip in Figure 8. The design points at the design pump shaft power (13.1 kW), marked by red dots and the highest efficiency

points (93.3%) marked by green squares also drawn on the normalized motor load and efficiency curves at the rated frequency (100%) in the same figure.

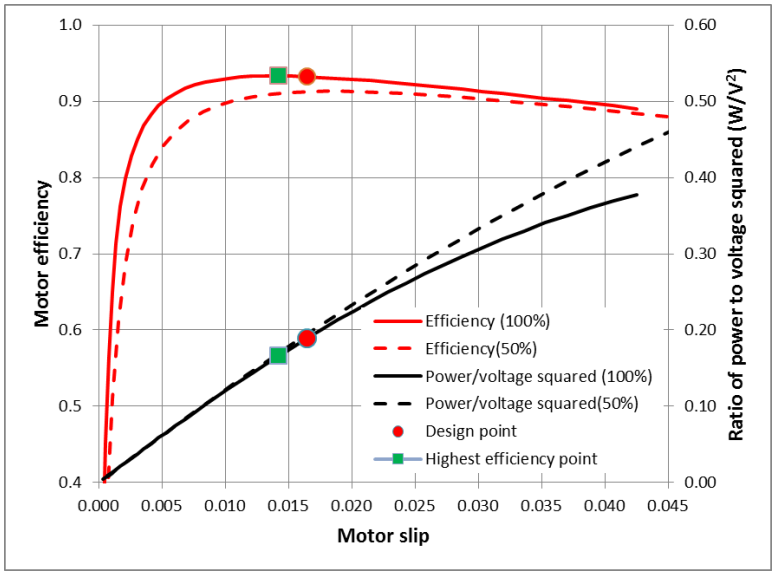

Figure 4-10 - Motor efficiency and normalized motor load versus motor slip.

Overall, the normalized motor load is approximately proportional to the motor slip, especially below the design points. Meanwhile the motor efficiency curve consists of three parts. The motor efficiency increases significantly as the motor slip increases in low motor slip ranges. Then it increases slightly and reaches to the highest efficiency point. After passing the highest efficiency point, it slightly decreases as the motor slip increases.

Even though the VFD voltage does not directly determine the motor efficiency, for a given motor load, the VFD voltage does change the normalized motor load, then change the motor slip along the normalized motor load-slip curve, and finally indirectly affect the motor efficiency along the motor efficiency-slip curve.

In general, the design points are on the right of the highest efficiency points, as shown in Figure 4-10. As the motor load decreases from the design points, the optimal voltage needs to remain at the rated voltage in order to reduce the normalized motor load and

consequently reduce the motor slip from the design points to the highest efficiency points. As a result, the optimal voltage remains the rated voltage as the motor load and relative VFD frequency just decrease from the design condition in Figure 6. When the motor operating points reach the highest efficiency points, the voltage has to track the motor load and relative VFD frequency to keep the actual motor slip always at the highest efficiency points. This is why that the optimal voltage tracks the reduced motor load and relative VFD frequency after the constant optimal voltage in high motor load and relative VFD frequency ranges in Figure 4-5.

Even though the design points are not the highest efficiency points, the design efficiency (93.2%) is really close to the highest efficiency (93.3%). For the fan and pump applications where the motor load is proportional to the cube of the motor speed, the voltage set by the relative frequency to the power of 1.5 will make the actual normalized motor load remain at the design normalized motor load. Consequently, the motor has the motor slip and efficiency equal to the design values.

$$\frac{W}{V_1^2} = \frac{W_d \cdot \omega^3}{\left(V_d \cdot \overline{f}^{1.5}\right)^2} = \frac{W_d}{V_d^2} \tag{4-17}$$

Similarly, for compressors where the motor load is proportional to the motor speed, the voltage set by the relative frequency to the power of 0.5 will remain the actual normalized motor load, slip and efficiency at the design values.

$$\frac{W}{V_1^2} = \frac{W_d \cdot \omega}{\left(V_d \cdot \overline{f}^{0.5}\right)^2} = \frac{W_d}{V_d^2} \tag{4-18}$$

Equations (4-17) and (4-18) explain that the voltage set by the ratio of voltage to relative frequency to the power of 1.5 is close to the optimal voltage for the cubic motor

loads and the voltage set by the ratio of voltage to relative frequency to the power of 0.5 is close to the optimal voltage for the linear motor loads.

On the other hand, the voltage set by the ratios recommended by the VFD manufacturers forces the motor operating points far away from the highest efficiency points. The voltage set by the squared ratio decreases faster than the voltage set the ratio of voltage to frequency to the power of 1.5 for the cubic motor loads as the motor load and VFD frequency decreases. Similarly, the voltage set by the linear ratio decreases faster than the voltage set the ratio of voltage to frequency to the power of 0.5 for the linear motor loads. As a result, the motor operating points move to the right and far away from the design points and consequently lead to in the motor efficiency degradation. Therefore, the current voltage-frequency settings recommended by VFD manufacturers are not optimal for both the cubic and linear relation applications.

4.2 Analytical approach to choose the optimal voltage to frequency ratio

4.2.1 Developing analytical relationship for different motor parameters

As mentioned before, A three-phase induction motor can be represented by three identical equivalent circuits. Figure 4-11 shows the schematics of an equivalent circuit with six circuit parameters, including stator winding resistance (R_1), rotor winding resistance (R_2), stator leakage reactance (X_1), rotor leakage reactance (X_2), magnetizing reactance (X_m), and core loss resistance (R_c), where the parameters of the secondary windings have been referred to the primary side.

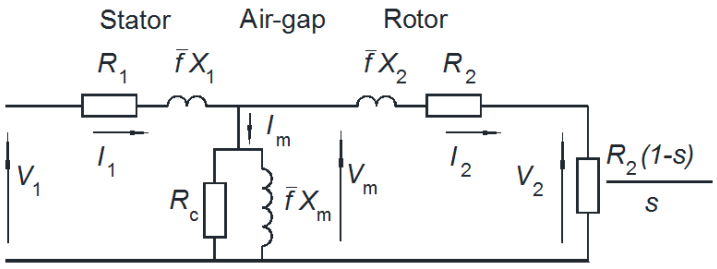

Figure 4-11 - Motor Equivalent Circuit with Six Parameters.

In the circuit, the reactance is proportional to the relative VFD frequency ($\bar{f}$), the ratio of actual frequency (f) to the rated frequency while the resistance is independent of the VFD frequency. Besides three resistances and three reactances, the load resistance is associated with the rotor winding resistance (R_2) and adjusted by the motor slip (s), the ratio of the difference between the synchronous speed and actual speed to the synchronous speed.

$$R_{load} = R_2 \frac{1-s}{s} \tag{4-19}$$

In general, the rotor winding resistance and leakage reactance are of similar values to the stator winding resistance and leakage reactance under the rated frequency. On the other hand, the magnetizing reactance is significantly higher than the stator and rotor impedances while the core loss resistance is much higher than the magnetizing reactance. Small motors typically have a design slip of 8% under the full-load condition while large motors are around 1% (Hughes 2006, Wildi 2002). As a result, the load resistance is much higher than the stator and rotor impedances.

Table 4-2 lists six circuit parameters in the equivalent circuit of a 60kW motor as well as the design slip and associated load resistance by Hughes (2006).

Table 4-2 - Equivalent circuit parameters.

Parameter (ohm)	Value
Stator winding resistance	0.2
Stator leakage reactance	1.0
Magnetizing reactance	40
Core loss resistance	250
Rotor winding resistance	0.3
Rotor leakage reactance	1.0
Slip	0.04
Load resistance	7.2

The losses of stator and rotor winding resistances correspond to the copper losses and the loss of core loss resistance corresponds to the core loss while the motor load is consumed by the load resistance if the mechanical losses are ignored.

Since the voltage drops across the stator and rotor will be small fractions of the supply voltage (V_1), the voltage (V_m) across the magnetizing branch including the magnetizing reactance and the core loss resistance, and the voltage (V_2) across the load resistance are almost equal to the supply voltage. In addition, since the slip has a small value, the rotor current (I_2) is approximately proportional to the product of the supply voltage and slip.

$$I_2 = \frac{V_2}{R_2 \dfrac{1-s}{s}} \propto sV_1 \tag{4-20}$$

The slip can be directly obtained by measuring the actual speed and can also be calculated by the motor load and supply voltage based on the relation that the motor load is approximately proportional to the slip and the supply voltage squared.

$$W = \frac{V_2^2}{R_2 \frac{1-s}{s}} \propto sV_1^2 \tag{4-21}$$

On the other hand, since the core loss resistance is much higher than the magnetizing reactance, the magnetizing current can be simplified as the current across the magnetizing reactance and is approximately proportional to the ratio of the supply voltage to the frequency.

$$I_m = \frac{V_m}{X_m} \propto \frac{V_1}{f} \tag{4-22}$$

For the motor defined in Table 4-2, the rotor and magnetizing currents are simulated under different conditions. Figure 4-12 shows the simulated rotor current versus the product of the slip and relative supply voltage with different ratios of the relative supply voltage to the relative frequency while Figure 4-13 shows the simulated magnetizing current versus the ratio of the relative supply voltage to the relative frequency with different products of the slip and relative supply voltage. The simulated currents in Figure 4-12 and Figure 4-13 undoubtedly validate Equations (4-20) and (4-22).

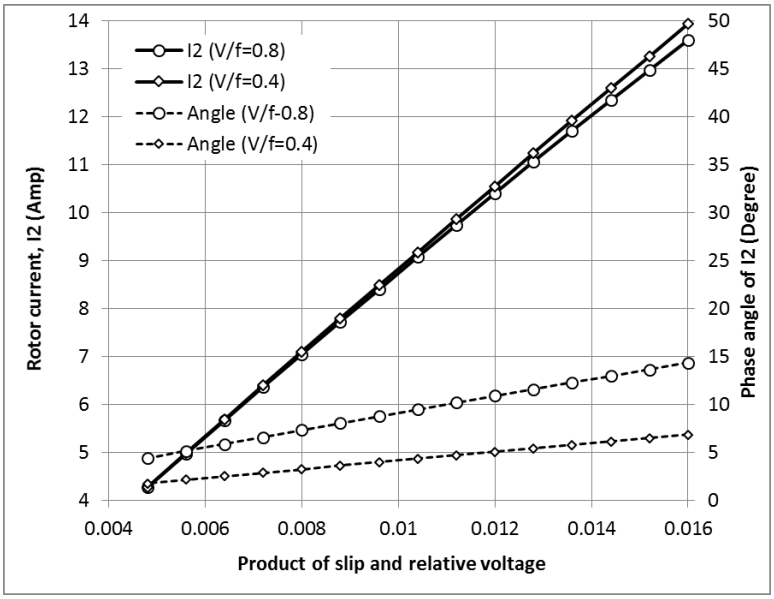

Figure 4-12 - Simulated rotor current versus product of slip and supply voltage.

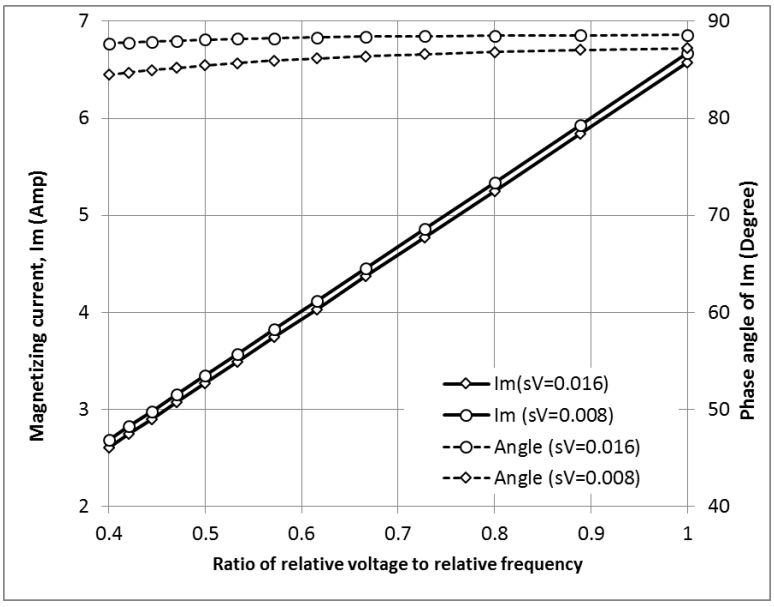

Figure 4-13 - Simulated magnetizing current versus ratio of voltage to frequency.

As discussed early, an AC induction motor develops torque (T) by the interaction of the magnetic flux (Φ) in iron cores produced by the stator and the induced currents (I_2) on the rotor.

$$T \propto \Phi \cdot I_2 \tag{4-23}$$

In fact, the stator current (I_1) is the sum of the magnetizing or flux-producing current (I_m) and the rotor or work-producing current (I_2). The work-producing current (I_2) is more or less in phase with the supply voltage (V_1), as shown in Figure 4-12, while the flux-producing current (I_m) lags the supply voltage (V_1) by almost 90º, as shown in Figure 4-13. The magnetic flux (Φ) is proportional to the flux-producing current and consequently proportional to the ratio of the supply voltage to the frequency.

$$\Phi \propto I_m \propto \frac{V_1}{f} \tag{4-24}$$

Therefore, the torque is proportional to the voltage to the frequency ratio and the rotor current.

$$T \propto \frac{V_1}{f} \cdot I_2 \tag{4-25a}$$

Moreover, the rotor current is defined by Equation (2), thus the torque is a function of the slip, supply voltage and frequency.

$$T \propto s\frac{V_1^2}{f} \tag{4-25b}$$

The magnitude of the flux-producing and work-producing currents determines the phase angle between the stator current (I_1) and supply voltage (V_1) and thus the power factor (PF) of the motor. Because of the high PF, the stator current is dominated by the work-producing current. In other words, the stator current is significantly impacted by the product of slip and voltage and insignificantly impacted by the ratio of voltage to frequency, as shown in Figure 4-14.

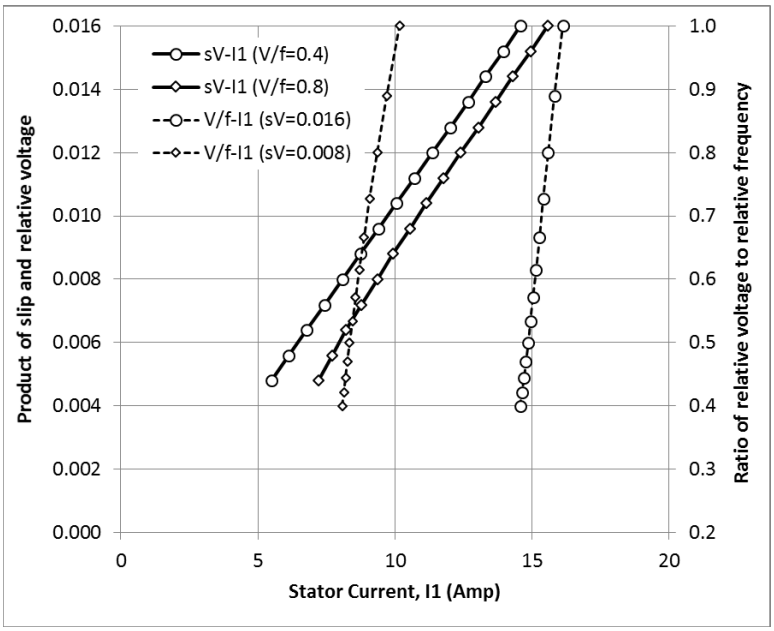

Figure 4-14 - Simulated stator current versus product of slip and voltage and ratio of voltage to frequency.

Similarly, the motor circuit impedance is more dominated by the slip, which can change the load resistance, than by the frequency, which can change reactance. Therefore motor efficiency depends significantly on the motor slip and insignificantly on the VFD frequency. Figure 5 shows the simulated motor efficiency versus the motor slip under relative frequency of 50% and 100%. The motor efficiency decreases as the slip decreases on the left side of the highest efficiency slip at Point B and as the slip increases on the right side.

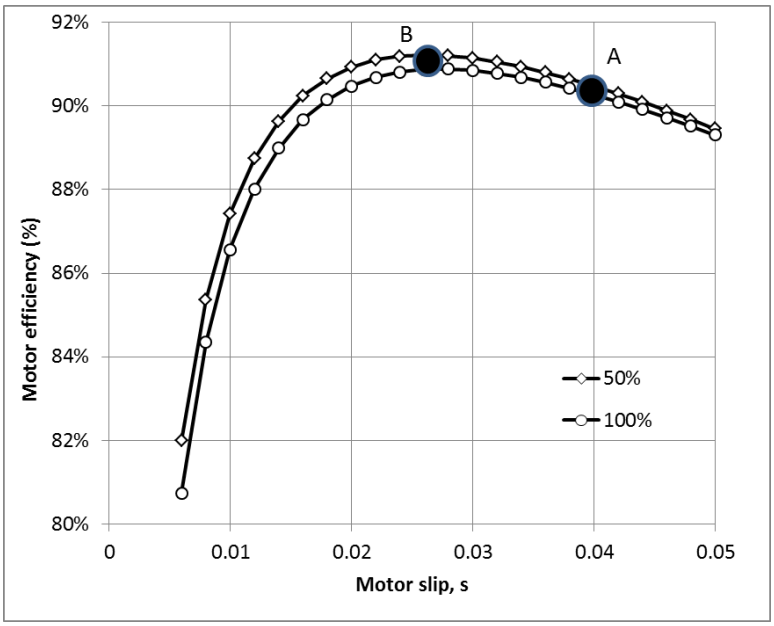

Figure 4-15 - Simulated motor efficiency versus motor slip at different frequencies.

As shown in Figure 4-15, the motor efficiency under the rated slip at Point A is close to the highest efficiency at Point B with a difference of 0.7%. If the slip is first adjusted from the rated slip at Point A to the highest efficiency slip at Point B and is then kept at the highest efficiency slip, the motor will always achieve the best energy performance. However, it cannot be implemented by a fixed ratio of voltage to frequency. On the other hand, the slip, which remains at the rated slip at Point A, can guarantee the motor operating at the efficiency close to the highest efficiency.

For positive displacement compressors, the torque is constant. Therefore, theoretically optimal voltage is proportional to the frequency to the power of ½ to maintain a constant slip based on Equation (4-25b).

$$V_1 \propto f^{1/2} \tag{4-26}$$

However, with the voltage controlled by Equation (4-26), the ratio of the voltage to the frequency under partial loads will be higher than the ratio of the rated voltage to the

rated frequency and consequently the magnetic flux will be saturated. To avoid the saturation, the actual voltage has to be proportional to the frequency to maintain constant magnetic flux.

$$V_1 \propto f \tag{4-27}$$

As a result, the slip increases as the frequency and voltage proportionally decreases. In other words, the liner ratio moves the slip to right far away from the highest efficiency slip and consequently slightly degrades the motor efficiency, as shown in Figure 4-15.

$$s \propto \frac{1}{V_1} \propto \frac{1}{f} \tag{4-28}$$

On the other hand, for centrifugal machines, the torque is proportional to the square of frequency.

$$T \propto f^2 \tag{4-29}$$

Therefore, optimal voltage is proportional to the frequency to the power of 3/2 to maintain a constant slip based on Equations (4-25b) and (4-29).

$$V_1 \propto f^{3/2} \tag{4-30}$$

Since the ratio of the voltage to the frequency under partial loads is always less than the ratio of the rated voltage to the rated frequency, the voltage controlled by Equation (4-30) will be optimal and can achieve higher motor efficiency without the saturation of the magnetic flux.

4.2.2 Assessment of existing voltage control

Unfortunately, the optimal voltage control defined by Equation (4-30) for centrifugal machines is not aware so far. On the other hand, government documentations and industrial standards provide two frustrated voltage controls.

The DOE (2004) and the U.S Department of Agriculture (USDA 2010) propose the linear ratio in their websites.

$$V_1 \propto f \tag{4-31}$$

The principle for the linear ratio is to keep the constant magnetic flux as the same as at the rated load to avoid the magnetic field saturation. As discussed previously, a constant V/f ratio typically provides motors with a higher amount of voltage than is required to control reduced load (Jeff 2011).

However, the linear ratio actually can improve the motor energy efficiency at higher frequency close to the rated frequency. It is readily derived that the slip is proportional to the voltage and frequency by substituting Equations (4-29) and (4-31) into Equation (4-25b).

$$s \propto V_1 \propto f \tag{4-32}$$

Equation (4-32) reveals that the slip decreases as the voltage and frequency decrease. As a result, the slip moves from the rated slip at Point A to the highest efficiency slip at Point B. However, when the slip reaches the highest efficiency point, the linear ratio will move the slip far away from the highest efficiency slip and a new ratio needs to be applied to keep the slip at the highest efficiency slip.

Besides the linear ratio, AHRI Standard 1210 (2017) recommends the squared ratio for centrifugal machines. Even though it did not give detailed reasons, some statements can still be found. The USDA (2010) claimed that VFDs keep a constant ratio of voltage and frequency so that motors have a constant current similar to full speed conditions. Danfoss (2017) stated that the liner V/f relationship keeps the current relatively constant.

All these statements apply an assumption that the rotor current is proportional to the ratio of voltage to frequency.

$$I_2 \propto \frac{V_1}{f} \tag{4-33}$$

With this assumption, the torque would be proportional to the square of the ratio of voltage to frequency. Roethemeyer and Yankaskas (1995) stated that the torque was considered to proportional to the V/f ratio squared. Consequently, the voltage would be proportional to the frequency to the power of 2 by substituting Equations (4-33) and (4-31) into Equation (4-25a).

$$V_1 \propto f^2 \tag{4-34}$$

If the voltage is controlled by Equation (4-34), the slip will be reversely proportional to frequency and voltage based on Equation (4-25b)

$$s \propto \frac{1}{f} \propto \frac{1}{V_1} \tag{4-35}$$

Equation (4-35) reveals that the slip increases as the voltage and frequency proportionally decreases. As a result, the slip moves to right from the rated slip at Point A and far away from the highest efficiency slip at Point B and the motor efficiency keeps decreasing as the frequency decreases.

In fact, the motor equivalent circuit has clearly derived that the rotor current is proportional to the voltage and independent with the frequency, descripted by Equation (4-20). Therefore, the assumption that the rotor current is proportional to the ratio of the voltage to frequency, defined by Equation (4-33), is unscientific and the associated voltage control (the voltage is controlled proportional to the square of the frequency)

defined by Equation (4-34), is incorrect and the resultant motor efficiency is not optimal due to excessive slip, controlled by Equation (4-35).

Two possibilities would result in this unscientific assumption. First, an incorrect sufficient condition would mistakenly come from its associated correct necessary condition. From Equation (4-25a), that the ratio of the voltage to the frequency is constant is necessary to that the rotor current is constant and the torque is constant. However, if the necessary condition was stated as the sufficient condition, that the ratio of the voltage to the frequency is constant would be sufficient to that the rotor current is constant and the torque is constant. In other words, the rotor current would be proportional to the ratio of voltage to frequency.

Second, the concepts of the stator, rotor and magnetizing current and the principle of torque development are not quite clear. As discussed previously, the stator current is the sum of the rotor current and magnetizing current and is also dominated by the rotor current. If the rotor current was treated as the same as the magnetizing current, the circuit impedance would be treated as the magnetizing reactance and consequently the current would be reversely proportional to the frequency. Chandran et al. (2011) stated that the motor impedance was considered to increase when the frequency increases.

4.3 Experiments

The purpose of the experiments are to demonstrate the impact of the voltage on the motor efficiency. Two fan-motor-VFD systems in a building cooling tower in a medical facility were selected for the experiment (Figure 4-16). The reason for selecting cooling tower fan is that the operaion of this system can be changed without any significant or dangerous effect on the facility mechanical systems.

Figure 4-16 - VFD experiment facility.

Two 15 kW (or 20 HP) 460 V three-phase induction motors provide power to the fans. The motors speeds are 1765 and 1770 rpm under the rated load while the synchronous speed is 1800 rpm at the rated frequency of 60 Hz. Two three-phase VFD was installed on the motor with the design output current of 31 Amps and the design output power of 15 kW. The VFD receives a 0-10 V output frequency command from a building automation system and has two 4-20 mA analog outputs from its control panel, which can be assigned to VFD output current, voltage, and power to the motor.

Some assumptions were applied in the experiment. First, since the rotor current is not measurable and the stator current is dominated by the rotor current, the stator current was measured to reflect the rotor current. Second, since the motor speed cannot be measured in the studied system, the slip was calculated from the motor load and voltage. Finally since the motor load is not measurable, the measurable VFD input power replaced the

motor load with assumptions that the VFD and motor efficiencies are relatively high and have minor variation.

A conventional power meter was installed on the power supply to the VFD to measure the system input power (W_{sys}) (Figure 4-17). The VFD output frequency and voltage and the motor current were obtained through the analog input and output on the VFD control panel.

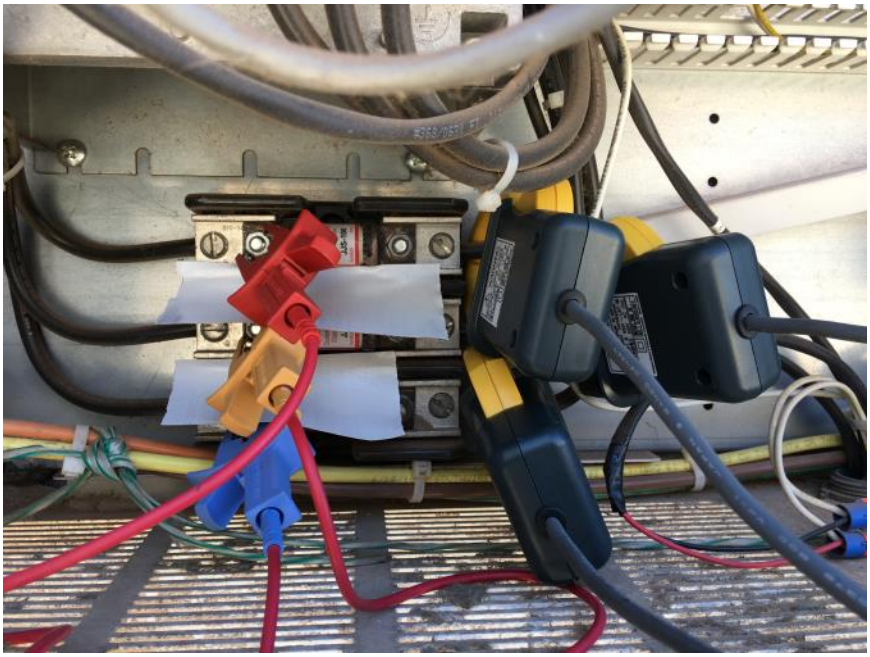

Figure 4-17 - power meter installed on the power supply to the VFD.

Figure 4-18 shows the relation between the voltage and frequency. Even though the flux optimizer was enable, it is hard to see the flux was optimized under dynamic load condition. Actually the voltage was controlled only based on the frequency independent with the motor load. The constant voltage to the frequency ratio was controlled at relative frequency higher than 39%. For the relative frequencies below 39% the squared ration is selected by flux optimizer.

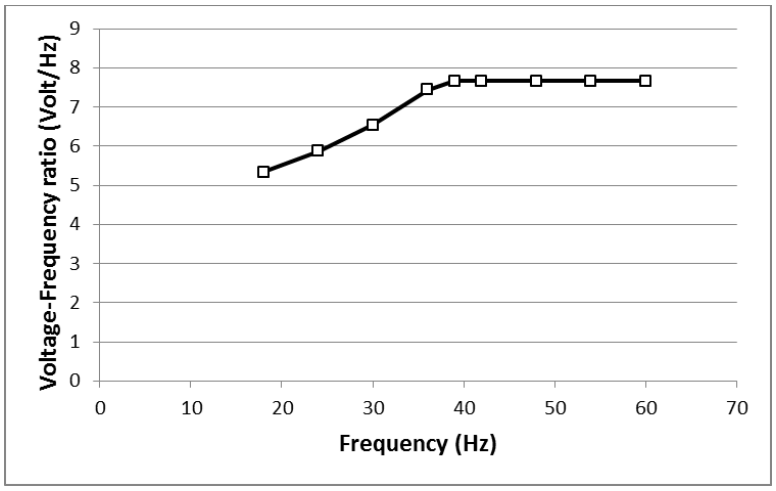

Figure 4-18 - Relation between VFD output voltage and frequency for flux optimizer mode.

For investigating the effects of different voltage to frequency ratios on system performance, 30 Hz frequency is chosed as the reference value and experiments conducted on the system with different voltages to be able to create different voltage to frequency ratios. For each voltage, data were logged for 10 minutes with 1 second time interval.

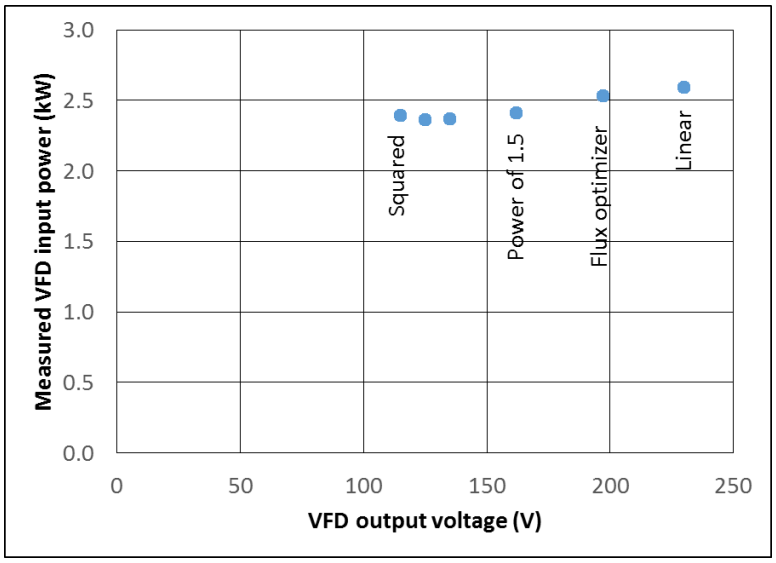

Figure 4-19 – Effects of different voltage to frequency ratios on VFD input power.

Figure 4-19 shows that the VFD input power changes as the voltage changes. Two manual points have been created to see how the power changes with respect to voltage between squared and 1.5 ratios. As it can be seen in the picture, Flux optimizer option does not provide the lowest power consumption. In this case, the squared ratios shows better performance than 1.5 but the optimal ratio is something between them. As mentioned in the section 4.2, choosing the optimal ratio depends on the motor design point on the efficiency curve.

4.4 Conclusions

The motor equivalent circuit method is applied to simulate the motor efficiency with different VFD voltage–frequency ratios for four different applications, including a pump with the ideal cubic load relation with the motor speed, a pump with two different pressure setpionts (25% and 50% of the design fan head respectively), and a compressor

with the ideal linear load relation with the motor speed. The simulation results in the following findings:

- The voltage-frequency ratios recommended by VFD manufacturers, the ratio of voltage to frequency to the power of 2 (the squared ratio) for applications with the cubic motor load-speed relation and the ratio of voltage to frequency (the linear ratio) for applications with the linear motor load-speed relation are not optimal.
- The optimal voltage remains at the rate voltage at the high frequency range and decreases as the frequency decreases in the low frequency ranges. The pressure setpiont impacts the optimal voltage and frequency ratio for pumps and fans with pressure control. The optimal voltage can improve the motor efficiency over all frequency ranges, for instant, by 3% at 40% of the rated frequency, over the ratios recommend by VFD manufacturers in both the cubic and linear relation applications.
- The motor efficiency with the ratio of voltage to frequency to the power of 1.5 is mostly close to the optimal efficiency for the ideal cubic motor load-speed relation applications while the motor efficiency with the ratio of voltage of frequency to the power of 0.5 cannot be applied to the motor because of oversaturation problem.

Experiments are performed on cooling tower fans to investigate the effects of different voltage to frequency ratio on the system power consumption. The results show that the Flux optimizer option is not always the best option and choosing the best settings depends on the motor design conditions.

Chapter 5: Fault detection and diagnosis

5.1 Pressure setpoint override fault

Faulty pressure transducer or unintentional overridden pressure setpoint can results in actual pressure much higher that required and consequently results in high pump power. In this case, the goal is to identify whether the system working based on the designed pressure setpoint or not.

The system schematic has been presented in Figure 5-1 the pump speed is moduatled to maintiant the pressure setpoint. A differential pressure sensor has been used for measuring pump head. Power has been measured using VFD in-situ power meter. In this study, virtual flow meter technology has been implemented to calculate the flow rate based on measured differential pressure and power (The details of this procedure can be found in (Wang et al. 2014)).

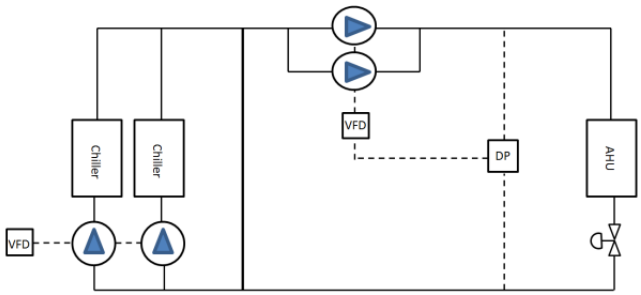

Figure 5-1 - schematic of the chilled water system.

The system control curve is determined by the pressure setpoint (H_{sp}). The system pressure drop includes the pressure drop upstream of the pressure sensor and the pressure drop downstream of the pressure sensor. Actually, the measured differential pressure

denotes the pressure drop downstream of the pressure sensor and is intentionally maintained at the pressure setpoint regardless of the flow rate. Therefore, the pressure drop downstream of the pressure sensor is approximately constant and equal to the pressure setpoint. On the other hand, the upstream of the pressure sensor does not have any modulation valves or dampers. Therefore, the pressure drop is proportional to the actual flow rate squared and is equal to the design system pressure drop or the design fan or pump head minus the pressure drop downstream of the pressure sensor at the design flow rate. The fan or pump head will overcome the system pressure drop.

$$H = H_{sp} + SQ^2 \tag{5-1}$$

.

It shoud be mentioned that Equation (5-1) can be used for turbulent flows which is the usual case in the HVAC applications.

Based on the measured head and flow rate, H_{sp} and S can be calculated using least square method.

$$X = \sum \Delta^2 = \sum (S{Q_i}^2 + H_{sp} - H_i)^2 \tag{5-2}$$

using least square method,

$$\frac{\partial x}{\partial S} = \sum 2\, Q_i^2\, (SQ_i^2 + H_{sp} - H_i) = 0 \tag{5-3}$$

$$\frac{\partial x}{\partial H_{sp}} = \sum 2\, (SQ_i^2 + H_{sp} - H_i) = 0 \tag{5-4}$$

Resulting in:

$$S\, \frac{\sum Q_i^4}{n} + H_{sp} \frac{\sum Q_i^2}{n} = \frac{\sum Q_i^2 H_i}{n} \tag{5-5}$$

$$S\, \frac{\sum Q_i^2}{n} + H_{sp} = \frac{\sum H_i}{n} \tag{5-6}$$

By solving the above equations simultaneously H_{sp} and S can be found.

Based on above equations, A method has been developed to track the H_{sp}. Assuming $\frac{\sum Q_i^4}{n} = x_{11,i}$, $\frac{\sum Q_i^2}{n} = x_{12,i}$, $\frac{\sum Q_i^2 H_i}{n} = y_{1,i}$, $\frac{\sum Q_i^2}{n} = x_{21,i}$, $1 = x_{22,i}$, $\frac{\sum H_i}{n} = y_{2,i}$, equations (5) and (6) can be rewritten as:

$$x_{11,i}S + x_{12,i}H_{sp} = y_{1,i} \tag{5-7}$$

$$x_{21,i}S + x_{22,i}H_{sp} = y_{2,i} \tag{5-8}$$

The following equations have been introduced to calculate the coeficients:

$$x_{11,i} = \frac{{Q_i}^4}{n} + \frac{1-n}{n} x_{11,i-1} \tag{5-9}$$

$$x_{12,i} = \frac{{Q_i}^2}{n} + \frac{1-n}{n} x_{12,i-1} \tag{5-10}$$

$$x_{21,i} = \frac{{Q_i}^2}{n} + \frac{1-n}{n} x_{21,i-1} \tag{5-11}$$

$$x_{22,i} = 1 \tag{5-12}$$

$$y_{1,i} = \frac{{Q_i}^2 H_i}{n} + \frac{1-n}{n} y_{1,i-1} \tag{5-13}$$

$$y_{2,i} = \frac{H_i}{n} + \frac{1-n}{n} y_{2,i-1} \tag{5-14}$$

The advantage of the developed method is that it can be easily implemented in BAS for pump speed control purpose.

5.2 Fan belt slippage fault

In AHUs, supply fan is controlled by the upstream pressure sensor. The pressure sensor sends signal to VFD to modulate the fan speed. The system schematic has been presented in Figure 5-2.

Fan belt slippage is one of the most common faults occurring in AHUs. This fault significantly decreases the efficiency of the fan resulting in more power consumption. If the fan belt is loose, the fan speed will be lower than what it should be. This phenomenon is more obvious when the speed is high.For identifying this fault, fan Head, Power and speed has been measured. Head has been measured using a differential pressure sensor. Power has been measured using VFD in-situ power meter. Speed has been calculated based on VFD frequency. A correlation has been derived between head, speed and power.

$$\frac{\sqrt[3]{W}}{\omega} = a\,\frac{\sqrt[2]{H}}{\omega} + b \tag{5-15}$$

The constants can be calculated using least square method based on measured data.

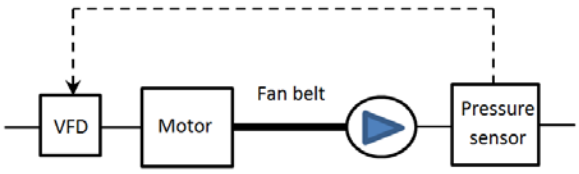

Figure 5-2 - Schematic of AHU supply fan.

5.3 Application and results

5.3.1 Pressure setpoint override fault

The chosen system for the case 1 is a primary-secondary chilled water system. The schematic of the system has been presented in the Figure 1. The secondary pumps are responsible for fixing the pressure set point. Any kind of wrong setting for defining set point can significantly affect the system performance. To develop a method for calculating the pressure set point, secondary pumps head, power and flow rate are

required. The experiments were conducted on a VFD-motor-pump system in a building chilled water distribution system on Tinker air force base in Oklahoma. Pump head and power have been measured for the period of 25 days. The measured data have been presented in the Figure 5-3. For this case, the Reynolds number has a order of 10^5; therefore the flow is fully turbulent.

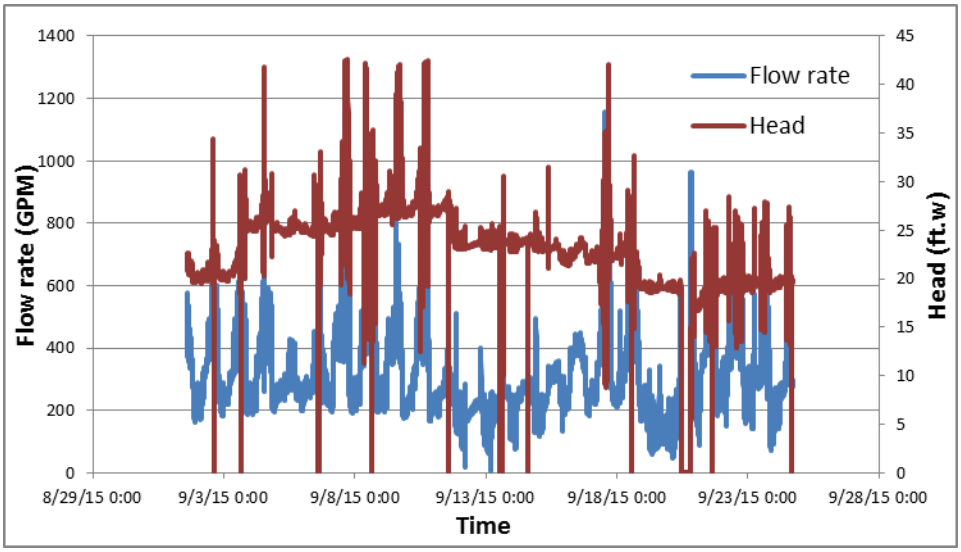

Figure 5-3 - Head and power measurements for chilled water pump.

The results for this case has been represented in Figure 5-4. The results show that the developed method can track the pressure set point. As it can be seen, hunting in measured data is resulting in hunting in calculated data. For the periods that the measured data profile is smooth, the calculated data can track them. If there is a fault in the system regarding pressure set point, Based on the developed method, the real pressure set point can be calculated and compared with the pressure set point which can be read from the BAS for fault identification purpose.

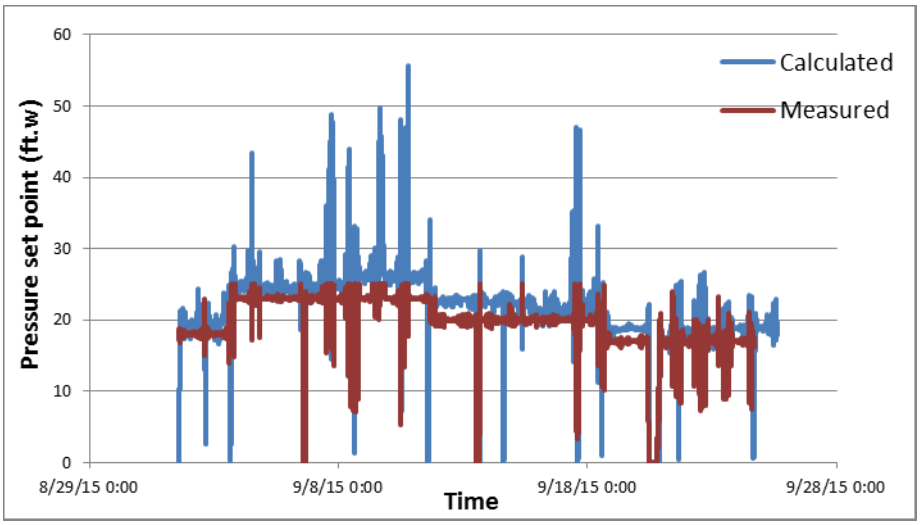

Figure 5-4 - calculated and measured pressure setpoint comparison in chilled water system.

5.3.2 Fan belt slippage fault

The chosen system for this fault is an AHU supply fan. The experiments were conducted on an AHU on Tinker air force base in Oklahoma. The fault was already in the system when the experiments were conducted. The data have been represented in Figure 5-5.

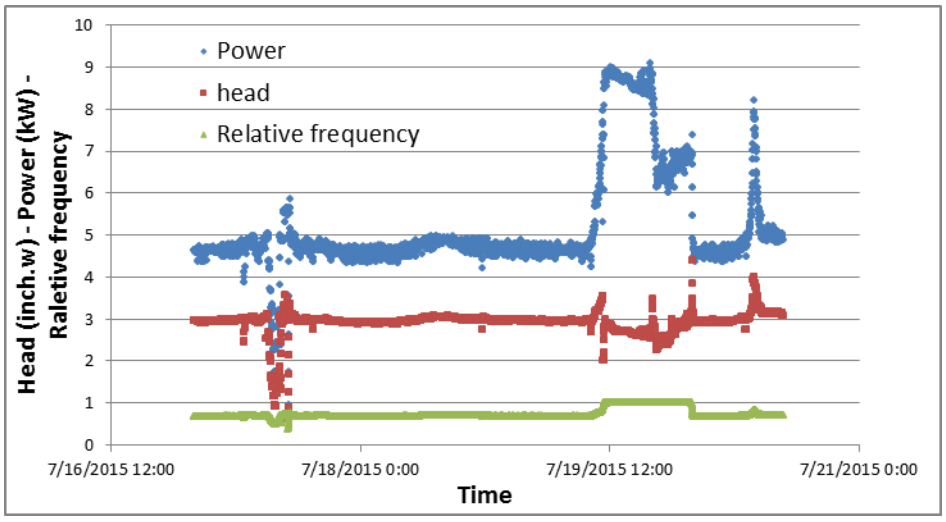

Figure 5-5 - Power, head and frequency measurement for AHU supply fan.

Figure 5-6 represents the projected power versus head. In this figure projected head and power have been calculated based on affinity laws for design speed. It can be seen that the chart has two part, one with higher power and head and the other part with lower power and head which the data from the latter part resemble fan belt slippage.

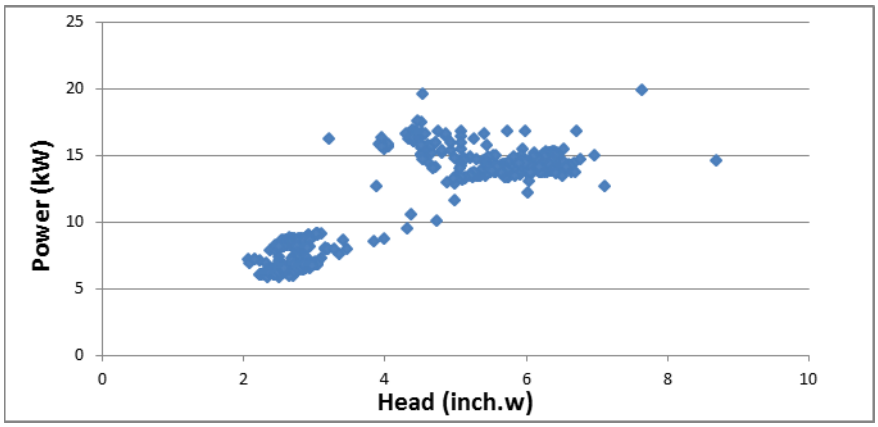

Figure 5-6 - Power versus head data for supply fan.

The results for this case have been presented in Figure 5-7. As it can be seen in the figure the calculated frequency is lower than measured frequency when the fault happens. Since the frequency is directly proportional to speed, the fault can be identified as fan belt slippage. It can be also observed that the fault occurs when the fan speed is high.

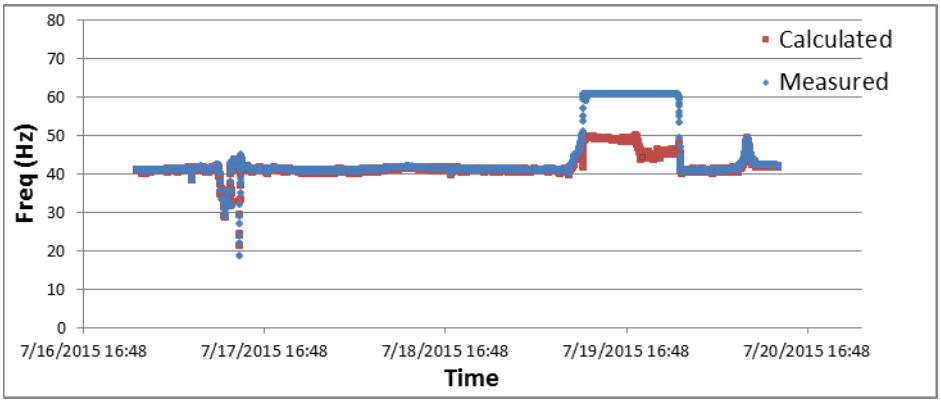

Figure 5-7 - calculated and measured frequency comparison for AHU supply fan.

Conclusion

Electric motors, which drive fans and pumps, provide the primary force to recirculate water and air in HVAC systems. In recent years, variable frequency drives (VFDs) have been extensively used in order to reduce the energy consumption of fans and pumps. In this study, the goal is to introduce methods to reduce the energy consumption and improve the performance of VFD-motor-pump/fan systems. Three enegy efficiency approaches is introduce in this work: Fault detection, VFD voltage to frequency ratio and virtual flowmeter (which is not an energy efficiency measure by itself but it is required for developing fault detection strategies.)

In this study, a hybrid approach has been used to identify two major faults in HVAC systems. The first fault, pressure set point override in chilled water pump system, has been identified using head and flow rate measurements. The results show that the developed automated calibration method can track the setpoint. The second fault, fan belt slippage, can be easily identified based on head, power and speed. For this case, a set of calibration data is needed.

The voltage-frequency ratios recommended by VFD manufacturers, the ratio of voltage to frequency to the power of 2 (the squared ratio) for applications with the cubic motor load-speed correlation is not optimal. The optimal voltage can improve the motor efficiency over all frequency ranges, for instant, by 3% at 40% of the rated frequency, over the ratios recommend by VFD manufacturers.

The motor efficiency with the ratio of voltage to frequency to the power of 1.5 is mostly close to the optimal efficiency for the ideal cubic motor load-speed correlation applications.

The explicit water flow correlation with the pump head and motor power was developed in association with pump and motor efficiencies. The motor efficiency is regressed as a function of motor power by consolidating multiple dependent factors and the pump efficiency is regressed as a function of the ratio of pump shaft power to pump head to the power of 1.5 by using the affinity laws.

References

ABB. 2011. Technical guide No. 7: Dimensioning of a drive system. New Berlin, United States.

AHRI. 2017. AHRI Certified Variable Frequency Drive (AHSI/AHRI 1210/1211) Operation Manual. Air-conditioning, heating and Refrigeration Institute, Arlington, Virginia.

Abdelaziz EA., Saidur R., Mekhilef S. 2011. A review on energy saving strategies in industrial sector. Renewable and Sustainable Energy Reviews; 15 pp.150–68.

AHRI. 2011. AHRI Standard 1210, Standard for Performance Rating of Variable Frequency Drives. Air-conditioning, Heating and Refrigeration Institute, Arlington, VA.

Andiroglu E., Wang G., Song L. 2013. Development of a virtual water flow meterusing pump head and motor power. Proceedings of Zero Energy MassCustomization Housing (ZEMCH2013) International Conference, Miami.

ASHRAE. 2012. 2012 ASHRAE HVAC System and Equipment Handbook, Centralized Cooling and Heating and Centrifugal Pumps. American Society of Heating, Refrigerating and Air-conditioning Engineers, Inc., Atlanta, GA.

ASHRAE. 2015. 2015 ASHRAE HVAC Applications Handbook, Supervisory Control Strategies and Optimization. American Society of Heating, Refrigerating and Air-conditioning Engineers, Inc., Atlanta, GA.

Austin H. 2009. Electric Motors and Drives: Fundamentals, Types and Application, third ed. Publisher Elsevier, India, ISBN 8131206688, pp. 305–323.

Burt C. M., Piao X., Gaudi F., Busch B., and Taufik N. F. N. 2008. Electric motor efficiency under variable frequencies and loads. Journal of Irrigation and Drainage Engineering 134(2), pp.129-136.

Carrier. 2005. Variable Frequency Drive. Carrier Corporation, Syracuse, New York.

Carling P., Haves P. 2001. Comparison of three fault detection methods based on field data of an air-handling unit. ASHRAE Transactions 108(1), pp. 904-924.

CEATI. 2000. Energy Efficient Reference Guide: Variable Frequency Drives. CEATI International, Montreal, QC, Canada.

Danfoss. 2014. Facts Worth Knowing about Frequency Converters. Danfoss, Nordborg, Denmark.

Dey A., Tripathi A., Singh B., Dwivedi B., and Chandra D. 2008. An improved model of a three phase induction motor incorporating the parameter variations. Electrical Power Quality and Utilization 14(1).

DOE. 2008. Improving Motor and Drive System Performance: A Sourcebook for Industry. U.S. Department of Energy, Office of Energy Efficiency and Renewable Energy, Washington, DC.

DOE. 2012. Energy Tips: Motor Systems (Tip Sheet #11). The U.S. Department of Energy Advanced Manufacturing Office of Energy Efficiency and Renewable Energy, Washington, DC.

DOE. 2012. Energy Tips: Motor Systems (Tip Sheet #3). The U.S. Department of Energy Advanced Manufacturing Office of Energy Efficiency and Renewable Energy, Washington, DC.

DOE. 2013. Energy Savings Potential and Opportunities for High-Efficiency Electric Motors in Residential and Commercial Equipment. The U.S. Department of Energy's Building Technologies Office, Washington, DC.

Du Z., Fan B., Chi J., Jin X. 2014. Sensor fault detection and its efficiency analysis in air handling unit using the combined neural networks. Energy and Buildings 72, pp.157-166.

Domijan A., Abu-aisheh A., and Czarkowski D. 1997. Efficiency and separation of losses of an induction motor and its adjustable-speed drive at different loading/speed combinations. ASHRAE Transactions 103(1), pp. 228-234.

Eaton. 2008. AC Drive Theory and Application. Eaton Corporation, Moon Township, PA, United States.

Eaton. 2013. M-Max Series Adjustable Frequency Drive. Eaton Corporation, Cleveland, United States

Fehr, J. 2011. ACH550 Flux Optimization White Paper. ABB, New Berlin, United States.

Gao X., McInerny S. A., and Kavanaugh S. P. 2001. Efficiencies of an 11.2 kW variable speed motor and drive. ASHRAE Transactions 107(2), pp. 259-265.

Gieras J.F., Wing M. 1997. Permanent Magnet Motor Technology, Design and Applications. NewYork: Marcel-Dekker.

Gragger J.V., Haumer A., Kral C., Pirker F.. 2008. Efficient Analysis of Harmonic Losses in PWM Voltage Source Induction Machine Drives with Modelica. Proceedings of the 6th Modelica Conference, Bielefeld, Germany.

House J. M., Lee W. Y., Shin D. R. 1999. Classification techniques for fault detection and diagnosis of an air-handling unit. ASHRAE Transactions105, pp. 1087-1100.

Hughes A. 2006. Electric Motors and Drives Fundamentals, Types and Applications, 3rd Edition. Burlington: Elsevier Ltd.

IEEE. 2004. IEEE Standard 112-2004, IEEE standard test procedure for polyphase induction motors and generators. New York: IEEE Power Engineering Society.

Krukowski A. and C. P. Wray. 2013. Standardizing Data for VFD Efficiency. ASHRAE Journal, June, pp. 16-26.

Lauro F., Moretti F., Capozzoli A., Khan I., Pizzuti S., Macas M., Panzieri S. 2014. Building fan coil electric consumption analysis with fuzzy approaches for fault detection and diagnosis. Energy Procedia 62, pp. 411-420.

Lee W. Y., House J. M., Kyong N. H. 2004. Subsystem level fault diagnosis of a building's air-handling unit using general regression neural networks. Applied Energy 77(2), pp. 153-170.

Liang J., Du R. 2007. Model-based fault detection and diagnosis of HVAC systems using support vector machine method. International Journal of refrigeration 30(6), pp. 1104-1114.

Liu M. 2003. Variable speed drive volumetric tracking for airflow control in variable air volume systems. Journal of Solar Energy Engineering 125 (3), pp. 318–323.

Liu G. 2006. Development and Applications of Fan Airflow Station and Pump WaterFlow Station in Heating, Ventilating and Air-Conditioning (HVAC) Systems. PhD dissertation of University of Nebraska – Lincoln.

Manz L. B., Morgan R. B. 1999. Mating new variable frequency drives to existing motors. Electrical Construction and Maintenance.

Montagud C., Corberán J. M., Montero Á. 2014. In situ optimization methodology forthe water circulation pumps frequency of ground source heat pump systems. Energy and Buildings 68, pp. 42-53.

Norford L. K., Wright J. A., Buswell R. A., Luo D., Klaassen C. J., Suby A. 2002. Demonstration of fault detection and diagnosis methods for air-handling units. HVAC&R Research 8(1), pp. 41-71.

Plessis G. E. D., Liebenberg L., Mathews E. H. 2013. The use of variable speed drives for cost-effective energy savings. Applied Energy 111, pp. 16-27.

Rishel J. B., Durkin T. H., and Kincaid B. L. 2006. HVAC pump handbook. Second Edition. New York City, NY: McGraw-Hill Professional.

Schneider Electric. 2012. Automation solution guide. Rueil-Malmaison, France.

Siemens. 2013. SINAMICS S120 Function Manual Drive Functions. Siemens AG Industry Sector Drive Technologies Motion Control Systems. Erlangen, Germany.

Song L., Wang G., Brambley M. R. 2013. Uncertainty analysis for a virtual flow meter using an air-handling unit chilled water valve. HVAC&R Research 19 (3), pp. 335-345.

WEG. 2010. Technical Guide - Induction Motors Fed by PWM Frequency Inverters. WEG Electric Corp., S.A. Brazil.

Wang G., Song L., Andiroglu E., Shim G. 2014. Investigations on a virtual airflow meter using projected motor and fan efficiencies. HVAC&R Research 20(2), pp. 1-10.

Wang G., Kiamehr K., L. Song. 2016. Development of a virtual pump water flow meter with an explicit expression of motor power and pump head. Energy and Buildings 117, pp. 63-70.

Wang G., Song L., Park L. 2013. Estimation of induction motor circuit parameters and efficiency under variable frequencies. ASHRAE Transactions, 119(2).

Wang S., Xiao F. 2004. AHU sensor fault diagnosis using principal component analysis method. Energy and Buildings 36(2), pp. 147-160.

Wang S., Zhou Q., Xiao F. 2010. A system-level fault detection and diagnosis strategy for HVAC systems involving sensor faults. Energy and Buildings 42(4), pp. 477-490.

Wang H. 2014. Water flow rate models based on the pipe resistance and pressure difference in multiple parallel chiller systems. Energy and Buildings 75, pp. 181-188.

Wildi, T. 2002. Electrical Machines, Drives and Power Systems, 5th Edition. Upper Saddle River: Pearson Education, Inc.